Basin Research IAS EAGE

Stratigraphic architecture of Solander Trough records Southern Ocean currents and subduction initiation beneath southwest New Zealand

Journal:	*Basin Research*
Manuscript ID	Draft
Manuscript Type:	Original Article
Date Submitted by the Author:	n/a

Complete List of Authors:	Patel, Jiten; Victoria University of Wellington, SGEES Sutherland, Rupert; Victoria University of Wellington, SGEES Gurnis, Michael; California Institute of Technology Division of Geological and Planetary Sciences, Division of Geological and Planetary Sciences Van Avendonk , Harm; University of Texas at Austin, Jackson School of Geosciences Gulick, Sean; University of Texas at Austin, UTIG Shuck, Brandon; University of Texas at Austin, Department of Geological Sciences Stock, Joann; California Institute of Technology Division of Geological and Planetary Sciences, Geological & Planetary Sciences Hightower, Erin; California Institute of Technology Division of Geological and Planetary Sciences, Division of Geological and Planetary Sciences

Keywords:	Antarctic Circumpolar Current, Subtropical Front, Puysegur, Fiordland, subduction-related basins, tectonics and sedimentation

Stratigraphic architecture of Solander Trough records Southern Ocean currents and subduction initiation beneath southwest New Zealand

Jiten Patel[1], Rupert Sutherland[1], Michael Gurnis[2], Harm Van Avendonk[3], Sean P.S. Gulick[3], Brandon Shuck[3], Joann Stock[2], Erin Hightower[2]

[1]SGEES, Victoria University of Wellington, PO Box 600, Wellington 6140, New Zealand.

[2] Seismological Laboratory, California Institute of Technology, Pasadena, CA 91125, USA.

[3] University of Texas Institute for Geophysics, Jackson School of Geosciences, Austin, TX 78758, USA

Highlights

- Basin architecture results from combined effects of subduction initiation, nearby continental collision, and development of the Antarctic Circumpolar Current.
- Growth of Puysegur Ridge, increase in sediment supply, and Tauru Fault inversion starting at ~17 Ma caused sediment accumulation in southern Solander Trough.
- Reverse faulting at 12 to 8 Ma was associated with a time of high stress, probably associated with subduction thrust propagation, and channelized sediment pathways.
- Reverse faulting and widening of southern Puysegur Ridge and Fiordland mountains at 5 to 0 Ma was associated with increased subduction maturity and sediment supply.

Keywords

Antarctic Circumpolar Current, Subtropical Front, Puysegur, Fiordland

Subduction-related basins, tectonics and sedimentation

Abstract

Solander Trough is in a region characterised by subduction initiation at the Pacific-Australian plate boundary, and has high biological productivity near the Subtropical Front at the northern edge of the Antarctic Circumpolar Current. Sedimentary architecture results from tectonic influences on accommodation space, sediment supply, and ocean currents (via physiography); and climate influence on ocean currents and biological productivity. We present the first seismic-stratigraphic analysis of Solander Trough that is based on high-fold seismic reflection data collected on voyage MGL1803 (SISIE). Solander Trough formed in the Eocene, but most sediment is younger than ~17 Ma, when we infer that Puysegur Ridge initially formed and sheltered Solander Trough from bottom currents, with contemporaneous tectonic activity causing terrigenous sediment supply to increase. A pulse of reverse faulting from 12 to 8 Ma caused inversion on the Tauru and Parara Faults, and likely was associated with a phase of lateral propagation of the subduction thrust. This phase of deformation created seabed topography that forced sediment pathways to become channelized into low points or antecedent gorges. Since 5 Ma, southern Puysegur Ridge and the Fiordland mountains have spread out towards the east, and structures such as Solander Anticline grew. This final phase of deformation likely reflects increasing maturity of the subduction thrust and reconfiguration of the hanging-wall to make space for subducted slab beneath. Simultaneously, the Snares Zone subsided, likely reflecting an increase in slab pull and reduction in interface strength. Solander Trough had anomalously high sedimentation rates because: (1) it is sheltered from bottom currents by Puysegur Ridge; and (2) it has a mountainous land area that supplies sediment to its northern end. The high-resolution record of climate and tectonics that Solander Trough contains may yield excellent sites for future scientific ocean drilling.

1 Introduction

The architecture of sedimentary basins results from an interplay between plate dynamic and climate processes. Solander Trough lies in a key region for understanding global tectonic and climate processes (Fig. 1), though before our study had only been explored with seismic-reflection methods at its northern margin, near the southern coast of New Zealand. Solander Trough lies adjacent to the Puysegur section of the active Pacific-Australia plate boundary, which is unique in being close to a transition from induced to self-sustaining subduction initiation (Gurnis, M. *et al.*, 2004). Solander Trough is swept by the largest oceanic current system, the northern edge of the Antarctic Circumpolar Current (ACC), which affects pelagic and hemi-pelagic sedimentation and the architecture of sediment gravity flow deposits. In this paper, we present a stratigraphic framework developed from the first regional survey of Solander Trough (Gurnis, M. *et al.*, 2019). We use it to describe how tectonics and climate have influenced basin architecture, and how sedimentary records from the region might provide new insights into tectonic mechanisms and climate history.

The ACC is driven by strong westerly winds and sinking of cold saline bottom water formed at the Antarctic margin (Rintoul, S. *et al.*, 2001). The current likely initiated at the start of the Oligocene in response to opening of the Tasmanian deep ocean gateway (Kennett, J. P., 1977; Carter, R. *et al.*, 2004), though opening of Drake Passage adjacent to the Antarctic Peninsula may also have played some role in its development (Barker, P. F. *et al.*, 2007). The strong current system reworks abyssal, bathyal, and shelf sediment eastward and northward over vast (>1000 km) distances south and east of New Zealand (Fig. 1) (Carter, L. *et al.*, 1996). The Subtropical Front, immediately southeast of New Zealand, represents a water mass boundary between ACC water derived from high latitude with waters pushed southward around the land area of New Zealand, and the location and amount of mixing varies between glacial and interglacial cycles (Carter, L. *et al.*, 2008; McCave, I. *et al.*, 2008; Bostock, H. C. *et al.*, 2015; Chiswell, S. M. *et al.*, 2015). Solander Basin is in a key region to record the history of ocean current variability.

The Australian plate is obliquely colliding with the Pacific plate at 36 mm/yr at Puysegur Trench (MORVEL, Fig. 1) (DeMets, C. *et al.*, 2010). A Wadati-Benioff zone of earthquake hypocentres to ~200 km depth is recognized beneath Fiordland (Fig. 1) (Eberhart-Phillips, D. & Reyners, M., 2001), and the first subduction-related volcano is exposed on Solander Island, where volcanic rocks yield Quaternary ages (Mortimer, N. *et al.*, 2013). Puysegur trench reaches maximum depths of ~6300 m, whereas Puysegur Ridge varies in depth from <150 m deep at its southern end to a maximum of ~2000 m in the Snares Zone, where flat-topped erosional morphology suggests geologically-recent subsidence from wave-base conditions (Collot, J.-Y. *et al.*, 1995). An axial valley along Puysegur Ridge is inferred to be the location of a major active strike-slip plate-boundary fault (Collot, J.-Y. *et al.*, 1995). Solander Trough lies east of Puysegur Ridge and contains a record of deformation and topography associated with plate boundary development (Fig. 1).

Solander Trough sedimentary basin architecture results from tectonic influence on accommodation space and ocean current systems (via physiography), and climate influence of ACC variability and biological productivity. Solander Trough has anomalously high sedimentation rates compared to immediately surrounding areas, because: (1) it is sheltered from strong bottom currents by Puysegur Ridge; and (2) it has a tectonically-active mountainous land area that supplies sediment at its northern end. The high-resolution record of climate and tectonics that the basin contains may in future yield excellent sites for scientific ocean drilling. Our study is the first to regionally image the sedimentary basin using high-fold seismic reflection methods, and hence we describe and map stratigraphic architecture for the first time.

2 Regional setting

Solander Trough is a bathymetric low and sedimentary depocentre, south of Fiordland, southwest New Zealand (Fig. 1). It is bound to the west by Puysegur Ridge and to the east by Campbell Plateau. Solander Trough gently slopes to the south and merges with relatively flat abyssal seafloor of Emerald Basin (Carter, L. & McCave, I., 1997), which is south of the surveyed area.

Southern Ocean waters in the study area include sub-tropical and subantarctic waters. The Subantarctic Front is a northern jet of the ACC that is deflected by Macquarie Ridge and Campbell Plateau (Carter, L. & McCave, I., 1997; Schuur, C. L. *et al.*, 1998). Farther north, elevated chlorophyll-a concentrations from photosynthesis in phytoplankton are observed along the Subtropical Front, which occurs due to mixing of relatively warm saline macronutrient-deficient micronutrient-rich subtropical water, with cool less-saline, macronutrient-rich micronutrient-poor subantarctic water (Deacon, G., 1982; Lorrey, A. M. *et al.*, 2012; Smith, R. O. *et al.*, 2013). This leads to high biological productivity around northern Solander Trough (Jitts, H., 1965; Hassler, C. S. *et al.*, 2014).

Solander Channel is the primary pathway for sediment gravity flows that descend along the axis of Solander Trough (Fig. 1). It extends from the Stewart Island continental shelf to beyond the study area, where it merges into relatively flat floor of Emerald Basin, south of Auckland Island (Schuur, C. L. *et al.*, 1998). Bathymetry data acquired during voyage MGL1803 (Gurnis, M. *et al.*, 2019) reveal that the channel is up to 220 m deeper than adjacent levees. Northern Solander Trough sediment is mainly composed of sand and mud, but carbonate content reaches 40-60% in southern parts of Solander Trough (Bostock, H. *et al.*, 2019). Solander Channel was most active during glacial low-stand conditions, when sediment was supplied to the shelf edge, and is inferred to have been inactive during the Holocene (Carter, L. *et al.*, 1996; Bostock, H. C. *et al.*, 2015; Jeromson, M. R., 2016). There is little sediment in Solander Trough at latitudes south of Auckland Island (transition with Emerald Basin, Fig. 1), due to strong currents of the Subantarctic Front, which penetrates Macquarie Ridge at ~53.5°S (Fig. 1) (Carter, L. & McCave, I., 1997; Bostock, H. *et al.*, 2019). Southeast Tasman Ocean Crust, which lies west of Puysegur Trench has only a thin veneer of sediment (Wood, R. A. *et al.*, 1996; Lamarche, G. *et al.*, 1997), due to strong erosive bottom currents and proximity to the Carbonate Compensation Depth.

Sedimentary basins at the northern end of Solander Trough have previously been mapped using petroleum industry seismic-reflection data and two wells: Parara-1 was drilled in 1975-1976 (Hunt International Petroleum Company 1976); and Solander-1 was drilled in 1985 (Engmann, L. A. & Fenton, P. H., 1986). From west to east, the Balleny, Solander, and Waiau basins are bound at their western margins by Puysegur Bank, the Hauroko Fault, and Solander Anticline, respectively (Turnbull, I. M. & Uruski, C., 1993). These structural highs were created by Neogene reverse faulting and folding, but there is clear stratigraphic evidence for reactivation of Eocene-Oligocene or/and Cretaceous normal faults (Sutherland, R. *et al.*, 2006). Puysegur Bank is actively uplifting and being eroded during sea-level low-stand conditions, but the southwestern end of the bank has deformed erosion surfaces that attest to a history of past uplift and relatively recent subsidence (Sutherland, R. *et al.*, 2006). The deepest erosion surfaces are found in the Snares Zone (Fig. 1), where they are up to 2000 m below sea level (Collot, J.-Y. *et al.*, 1995; Lamarche, G. & Lebrun, J.-F., 2000). Farther south, Puysegur Ridge has an eroded crest that is at ~125 m depth at its southern end, consistent with sea-level low-stand erosion at 20 ka, but erosion surfaces have subsided at the northern end of Puysegur Ridge, where they are ~625 m depth (Collot, J.-Y. *et al.*, 1995).

Fiordland is composed of plutonic and meta-plutonic rocks, with lesser amounts of metasedimentary rocks, and deformed Cenozoic sedimentary basins along its eastern and southern margins (Turnbull, I. M. *et al.*, 2010). Onshore Cenozoic basins adjacent to Fiordland attest to a history of Eocene-Oligocene trans-tension, followed by a complex history of strike-slip motion and Neogene basin inversion associated with a coarsening-upward transition from marine mudstone, to turbidites, to marine and terrestrial conglomerates (Norris, R. *et al.*, 1978; Norris, R. & Turnbull, I., 1993; Turnbull, I. M. & Uruski, C., 1993). In some places, Cenozoic basins are superimposed on Cretaceous basins that record rifting from Gondwana and subsequent subsidence (Norris, R. *et al.*, 1978; Norris, R. & Turnbull, I., 1993; Turnbull, I. M. & Uruski, C., 1993). The elevated topography of Fiordland mountains (many peaks 1000-2000 m above sea level) and hence exhumation and relevance as a sediment source is related to dynamic forces associated with subduction initiation (House, M. A. *et al.*, 2002). Themochronology data from Fiordland reveal that: exhumation started locally in the southwest corner of Fiordland at ~25-15 Ma; the zone of exhumation spread northward up the western margin of Fiordland during the interval 15-5 Ma; and then the zone of exhumation broadened eastward since 5 Ma (Sutherland, R. *et al.*, 2009; Klepeis, K. *et al.*, 2019).

Subduction related volcanism is represented by Solander Island and Little Solander Island (Fig. 1), which are extinct adakitic (Reay, A. & Parkinson, D., 1997) volcanic remnants of a larger edifice (Mortimer, N. *et al.*, 2013). Adakitic chemistry is classically interpreted as melting of a young subducted slab (e.g. as found at Adak Island in the Aleutian arc) and is also associated with highly oblique subduction, and both factors are present in our case, where young (<40 Ma) Southeast Tasman Ocean Crust is being obliquely subducted (Lamarche, G. *et al.*, 1997), but a range of other explanations might also exist that might shed new light on how the mantle wedge is metasomatised during subduction initiation (Castillo, P. R., 2012). Mortimer, N. *et al.* (2013) determined the age of volcanism at Solander Island to be 350–100 ka, and at Little Solander Island to be 50–20 ka. Additional small volcanic features are evident in bathymetric maps and on seismic-reflection data farther west at the southern tip of Neogene Hauroko Fault activity, but these features remain unsampled (Lamarche, G. & Lebrun, J.-F., 2000; Sutherland, R. *et al.*, 2006).

3 Data

Petroleum exploration data from the northern end of Solander Trough were acquired in the 1970s and 1980s and are now publicly available under New Zealand's open-file system (the 'Exploration Database' at nzpam.govt.nz). The Parara-1 well is near the southern extent of this dataset and is our most useful stratigraphic tie (Hunt International Petroleum Company 1976).

A single seismic line that crosses the region was acquired with an 8495 in^3 (0.139 m^3) air-gun source just south of Stewart Island in 1996 using *RV Maurice Ewing* (voyage EW9601) (Melhuish, A. *et al.*, 1999; Sutherland, R. & Melhuish, A., 2000). We edited and reprocessed original field data for our work (Table 1). The reprocessed data are available via New Zealand's open-file system (data.nzpam.govt.nz) and the Marine Geoscience Data System (Academic Seismic Portal, www.marine-geo.org). [Aside: we will lodge the reprocessed EW9601 data after the paper is accepted, so that a correct reference can be inserted into the headers and documentation]

The South Island Subduction Initiation Experiment (SISIE) involved acquisition of 2D seismic reflection and refraction data, including ocean-bottom seismometer observations, during *RV Marcus Langseth* voyage MGL1803 in 2018 (Gurnis, M. *et al.*, 2019). Seismic reflection data were acquired with a 6600 in^3 (0.108 m^3) source and streamer that varied in length between 4 and 12.6 km. Shot spacing was 50 m and streamer depth was between 10 and 18 m, depending on swell conditions. Our seismic processing workflow consisted of trace editing, filtering, velocity analysis, radon multiple suppression, and post-stack f-k migration (Table 1). The resulting post-stack time images, in combination with a seismic-well tie age model, allow us to regionally interpret the stratigraphic evolution of Solander Trough.

4 Seismic stratigraphy

A seismic stratigraphy is developed, based on subdivision into genetically-related units inferred from internal seismic-reflection character, stratal stacking pattern, and termination relationships at bounding reflectors. We do not assume that sequence or megasequence boundaries are directly linked to sea level variations (Vail, P. *et al.*, 1977), but more simply that sequence definition is allostratigraphic in nature and reflects a variable combination of sediment supply, climate, and tectonics; and this is appropriate because most of the region we map is in a bathyal slope environment far from a shallow shelf (Catuneanu, O. *et al.*, 2009).

Our primary tie for sequence and megasequence boundaries is the Parara-1 well, which penetrates a thick sequence of Neogene marine mudstone and sandstone; a condensed sequence of Paleogene upward-fining coaly sandstone, mudstone, and limestone; and a basal sandy conglomerate that is undated, but could be of Cretaceous or Paleogene age (Hunt International Petroleum Company 1976) (details in section 5).

Sedimentary and structural barriers affect continuity of mapping, and hence correlations based on stratigraphic position and seismic-reflection character are required to make regional interpretations. In most cases this is straightforward, but the Tauru Fault is a major structure south of the Parara-1 borehole that introduces significant uncertainty in correlation, due to large footwall accommodation space that was created during Neogene reverse fault activity that created Tauru High (Sutherland, R. & Melhuish, A., 2000). Therefore, we define separate stratigraphic units in sub-basins north and south of the Tauru Fault, and then discuss our preferred correlation. We use nomenclature that makes this clear, e.g., SLN3-2 refers to a unit in northern Solander sub-basin, megasequence 3, sequence 2. We use prefix SLS for units south of the Tauru Fault. We abbreviate survey name MGL1803 to M18 (in line with convention used for S86).

4.1 SLN1-1

Internal reflections have low-continuity high-to-moderate amplitude and fan outwards towards the Tauru Fault and Parara Fault (Fig. 2). The basal surface has variable amplitude, moderate or low continuity, and local onlap. The inferred dips of the Tauru Fault and Parara Fault, in combination with thickness variation and onlap, implies normal faulting was occurring during deposition of SLN1-1.

4.2 SLN2-1

Internal reflections are parallel, have moderate-to-low amplitude, and high continuity. SLN2-1 thins toward the Tauru Fault and is absent from ~CDP 4000–12400 on line M18-17c (Fig. 2). On line S86-34 (Fig. 2), SLN2-1 thickens westward of the Parara Anticline, in contrast to underlying SLN1-1, which is condensed and slightly thickens in the opposite direction (Fig. 2A ~CDP 0–3500; Fig. 2B, ~CDP 0–750).

SLN2-1 strata onlap basement north of Tauru High and on the southern limb of Parara Anticline (Fig. 2). On the northern flank of Tauru High, strata onlap a high-continuity high-amplitude positive-polarity reflector at the top of SLN1-1. Further onlap of SLN2-1 onto this reflector occurs north of Parara Anticline at ~CDP 14400 (line M18-17c, Fig. 2). However, this reflector downlaps basement on the southern limb of the anticline, where a relatively planar surface from CDP 10000–12500 implies erosion of strata down to basement, possibly due to uplift of the footwall of the fault during its extensional phase (Sutherland, R. *et al.*, 2006). SLN2-1 strata onlap this basal reflector west of Parara Anticline and downlap it east of Parara Anticline (line S86-34, Fig. 2). On line S86-34, the basal reflector is mapped as a high-continuity high-amplitude reflector. The relatively uniform thickness of megasequence

SLN2 across Parara Anticline suggests the Parara Fault was not active during deposition.

Onlap and downlap of SLN2-1 strata onto the basal reflector and significant thickening towards Solander Anticline, suggests accommodation space was being created by movement on the Solander Fault (we assume the anticline results from fault movement at depth), or another fault farther west, during deposition of SLN2-1, or that accommodation space created earlier remained under-filled.

4.3 SLN2-2

Internal reflections have moderate-to-low amplitude, variable continuity, and are parallel to each other but locally folded (Fig. 2). On the northern flank of Tauru High (line M18-17c, Fig. 2), SLN2-2 onlaps a continuous high-amplitude reverse-polarity reflector. SLN2-2 strata onlap this basal reflector west of Parara Anticline (line S86-34, Fig. 2), and are conformable to the east. On line M18-17c, north of ~CDP 4200, SLN2-2 strata onlap basement. Similar to SLN2-1, SLN2-2 thickens north of Tauru High and Parara Anticline, which suggests an increase in sediment flux from the north during accumulation of megasequence SLN2, and initial inversion of the Tauru Fault.

4.4 SLN3-1

Internal reflections have moderate-to-high amplitude and low-to-moderate continuity between Tauru High and Parara Anticline. A paleochannel that originates at the base of the sequence is identified at ~CDP 5500 on line M18-17c (Fig. 2), based on stratal truncations and local differences in amplitude. North of this paleochannel, strata are continuous and parallel. SLN3-1 is a relatively thin unit on line M18-17c, though thickening occurs adjacent to Tauru High (CDP 1350–3800, Fig. 2A). Thickness variations are evident at Parara-1, though interpretation is complicated by the significant paleochannel at CDP ~12000 on line M18-17c (Fig. 2A). On line S86-34 (Fig. 2), strata are more continuous and parallel, and downlap or onlap the basal surface. SLN3-1 strata onlap the northern flank of Tauru High and a basement high at CDP 8400 line M18-17c (Fig. 2A). The basal surface of SLN3-1 marks the onset of channel systems north of Tauru High (~CDP 4700–7000, Fig. 2) and adjacent to Parara Anticline. We interpret the SLN3-1 thickness variations and localization of deposition into a channel system as recording the growth of seafloor topography caused by folding and reverse faulting that guided sediment transport pathways.

4.5 SLN3-2

Internal reflections have low-to-moderate amplitude and high continuity. Slight thickening north (line M18-17c, Fig. 2) and west (line S86-34, Fig. 2) of Parara Anticline is observed. The basal boundary with SLN3-1 becomes indistinct in paleochannels (Fig. 2). Onlap onto a high-amplitude basal surface leads to assignment as a sequence boundary. We assign this unit to megasequence SLN3, because thickness variations adjacent to Parara-1 have similar architecture to SLN3-1. Anticline growth may have continued during deposition of SLN3-2, but it is plausible (likely?) that fault movement ceased during deposition of SLN3-1, leaving relict topography that influenced the facies and architecture of unit SLN3-2.

4.6 SLN4-1

Internal reflections have variable amplitude and high continuity. The unit thickens north of Tauru High and south of Parara Anticline (line M18-17c, Fig. 2), and it pinches out west of Parara Anticline on line S86-34 (Fig. 2). On line M18-17c, a paleochannel feature is identified at CDP 11500 (approx. 1.5 s TWT, Fig. 2A), and similar high-amplitude reflections at CDP 1500 (1.25 s TWT) on line S86-34 may be part of the same channel system (Fig. 2B). An active channel, visible in seafloor morphology, is inferred to be the modern depositional analogue. East of Solander Anticline (line S86-34, Fig. 2), SLN4-1 strata onlap a low-continuity moderate-to-low amplitude reflector. We infer that folding at Solander Anticline caused tilting and onlap during deposition of SLN4-1, and hence deposition became localized into a channel, while condensed pelagic or hemi-pelagic deposition occurred near the crest of Solander Anticline (Fig. 2).

4.7 SLN4-2

SLN4-2 deposits underlying the modern continental slope between the southern end of line M18-17c and Parara-1 are of variable amplitude and high continuity (Fig. 2). By comparison, below the modern continental shelf, reflectors have moderate amplitude and low-to-moderate continuity. The unit is truncated by a modern channel at CDP 1700-1920 on line S86-34 (Fig. 2B), and is truncated by a modern channel at CDP 2500 on line M18-17c (Fig. 2A). These are main tributaries of Solander Channel, which can be traced >300 km southward using our dataset (Fig. 1). SLN4-2 is thickest to the north and east of Parara Anticline and it thins southward towards Tauru High and westward toward Solander Anticline (Fig. 2). Minor onlap occurs onto the basal surface, which can be mapped regionally.

4.8 SLN4-3

SLN4-3 is differentiated from underlying SLN4-2 on the basis of higher continuity and lower amplitude reflectors. It contains channels and levees that include active features evident in seafloor morphology. Continental slope deposits of SLN4-2 are imaged as continuous low-amplitude parallel reflectors that transition into moderate-amplitude stacked clinoforms beneath the continental shelf (north of CDP 12500 in Fig. 2A; east of CDP 800 in Fig. 2B). SLN4-3 thins to the south and west.

4.9 SLS1-1

Internal reflections have low amplitude, low-to-moderate continuity, are locally folded on line M18-17b at ~CDP 8000, and onlap basement south of Tauru High (Fig. 3). The top of SLS1-1 immediately south of Tauru High is an unconformity with downlap of overlying reflectors, which have higher amplitude and continuity (M18-17b, Fig. 3). The intersection of line M18-17b and M18-01 occurs on a basement high with minimal sedimentary cover, so the top of SLS1-1 farther south is based on continuity and thickness of younger units, and the character of reflections in SLS1-1: low-to-moderate amplitude and moderate continuity.

Farther south, on line M18-23ab, SLS1-1 comprises moderate-to-high amplitude reflections with high continuity. Correlation and mapping between lines M18-01, M18-23ab, and M18-14 (Fig. 4) was on the basis of seismic-reflection character, despite basement topography (~CDP 28800–34000 on line M18-23ab; and ~CDP 4200–6500 on line M18-14). SLS1-1 is variable in thickness and thickens locally in depressions (e.g. CDP 35500, line M18-23ab; and ~CDP 7800, line M18-14).

The reflector at the base of SLS1-1 (seismic basement) has low continuity, moderate amplitude and positive polarity. Basement is poorly imaged within Tauru High (M18-17b ~CDP 9500–11500, Fig. 3), though it is distinguished from overlying strata on the basis of internal reflection characteristics. SLS1-1 onlaps basement on all southern lines.

4.10 SLS2-1

Internal reflections have low-to-moderate amplitude and low-to-moderate continuity on line M18-17b (Fig. 3). The base of the unit is uncertain on line M18-01 (Fig. 3), due to correlation uncertainty with line M18-17b, but reflections on M18-01 have high continuity and low-to-moderate amplitude. SLS2-1 can be mapped southward along line M18-23ab, where reflections have moderate-to-high continuity and low-to-moderate amplitude. SLS2-1 can be mapped west onto line M18-14 (Fig. 4), where reflections are continuous and low-to-moderate amplitude and the sequence is folded on the eastern flank of Puysegur Ridge from ~CDP 11000–13750 (Fig. 4B). SLS2-1 is thickest immediately south of Tauru High (Fig. 3), and thins towards basement topography. Onlap occurs onto volcanic or basement highs on lines M18-23ab and M18-14 (Fig. 4). SLS2-1 downlaps its basal surface just south of Tauru

High (Fig. 3), suggesting sediment supply from the north.

4.11 SLS2-2

Internal reflections have low-to-moderate amplitude and high continuity. SLS2-2 downlaps onto a continuous high-amplitude reverse-polarity basal reflector adjacent to Tauru High (~CDP 9000, line M18-17b, Fig. 3A). Onlap onto basement is observed on all lines. The basal surface is assigned sequence boundary status, because overlying strata are conformable everywhere, except for local downlap on line M18-17b near Tauru High.

4.12 SLS2-3

Internal reflections have low-to-moderate amplitude and high continuity. SLS2-3 is relatively thin on lines M18-17b and M18-01 (Fig. 3), but thickens southward on line M18-23ab. It thickens towards Puysegur Ridge on line M18-14. The basal surface is mostly conformable with underlying units, but onlap is observed at ~CDP 9500 on line M18-17b, on line M18-01 (Fig. 3), and at ~CDP 15000 on line M18-23ab. SLS2-3 onlaps basement to the south of Tauru High on line M18-17b, and to the west of the basin on line M18-01, and on line M18-23ab (CDP 4600–9300). The basal surface is picked on the basis of high continuity and differences in stacking patterns within units above (SLS2-4) and below (SLS2-2).

4.13 SLS2-4

Internal reflections have low-to-moderate amplitude and high continuity, but local channels are interpreted from amplitude and termination relationships (Fig. 3). SLS2-4 is thickest on the east of line M18-01, and gently thins southward along the axis of Solander Trough (line M18-23ab) and eastward onto Puysegur Ridge. SLS2-4 reflectors are mostly conformable with the basal reflector, which is continuous and has moderate-to-high amplitude. Minor onlap occurs on line M18-01 (CDP 37500, Fig. 3) and east of Puysegur Ridge (line M18-14, CDP 11500, Fig. 4B), and basement onlap is clear in the south (Figs. 3 & 4).

4.14 SLS3-1

Two facies are identified (Fig. 3). SLS3-1a contains low-to-moderate amplitude reflectors with moderate-to-high continuity, whereas SLS3-1b consists of higher amplitude reflections with lower continuity. SLS3-1a is most widely recognized and is the main facies in the southern part of the region, where continuity is highest. Channel axis deposits are inferred from localized but vertically-stacked high-amplitude reflectors, and on line M18-23ab the steep channel margins lead to broken continuity of reflectors. Paleochannel locations can be linked upwards to seabed expression (e.g. Fig. 3).

Basal onlap is identified east of Puysegur Ridge on line M18-14 (Fig. 4), on line M18-23ab in the basin axis (~CDP 23000 and 32600), and farther west on line M18-01 (~CDP 35750 and CDP 41000–41500) (Fig. 3). The unit is of relatively consistent thickness, but thins onto Puysegur Ridge on line M18-14 (Fig. 4). Megasequence status is justified from onlap and thickness variations that show SLS3-1 records growth of southern Puysegur Ridge. The significant channel and levee deposits within this unit are recognized up to the seabed and provide evidence for a similar sedimentary regime to that of the late Quaternary throughout the unit.

4.15 SLS3-2

Internal reflections have low-to-moderate amplitude and high continuity, but channels, drift deposits, and local scouring is observed (e.g. the moat next to Puysegur Ridge). The unit has variable thickness across the southern study area. Basal onlap onto a continuous, low amplitude, reverse polarity reflector is observed on line M18-14 (Fig. 4), and line M18-01 (Fig. 3). The onlap and dip of reflectors shows that little or no growth of southern Puysegur Ridge occurred during deposition of SLS3-2 (Fig. 4).

5 Parara Anticline

5.1 Parara-1 borehole

The Parara-1 borehole was drilled in 1975-1976 and is located 22 km ESE of Solander Island (Fig. 1) in 148 m water depth (PPL 38206, Hunt International Petroleum Company 1976). The petroleum exploration target was the crest of Parara Anticline, which has ~2.1 km of vertical closure (Fig. 2). Parara Anticline is inferred to have formed by Neogene reactivation of a Paleogene or Cretaceous extensional fault (e.g. Turnbull, I. M. & Uruski, C., 1993; Sutherland, R. *et al.*, 2006). A summary of drilling results and local seismic interpretation is shown in Figure 5. Checkshot data give accurate conversion of two-way time to depth at Parara-1 (Tables 2, 3 and 4).

The Pleistocene to mid Miocene stratigraphy of Parara-1 comprises outer shelf to bathyal clay and silt with rare fine sand. From the mid Miocene to Oligocene, strata are fine-grained sandy shelf deposits with calcareous fossils and some limestone. Older strata are terrestrial sands, silt, and coal. The base of the borehole sampled amphibolite facies metamorphic basement rock. No significant petroleum was encountered and the well was plugged and abandoned at 3800.5 m below Kelly Bushing (BKB), which was the local rig vertical datum at 31.1 m above mean sea level (MSL).

5.2 Eocene normal faulting

SLN1-1 fanning growth strata provide evidence for an initial phase of extension on the Parara Fault (Fig. 2). SLN1-1 reaches a maximum thickness of ~950 m adjacent to the Parara Fault, with thinning and onlap onto basement nearby. The top of unit SLN1-1 correlates with a downhole lithological change in Parara-1 from condensed mudstone and limestone to coaly sandstone. Significant downhole changes at the megasequence boundary (top SLN1) are confirmed by gamma ray and resistivity logs.

The upper part of SLN1-1 is dated from pollen to be ~46-37 Ma, but the lower part is poorly dated. Phases of Cretaceous and Eocene normal faulting are regionally inferred from onshore stratigraphy and structural mapping (Norris, R. & Turnbull, I., 1993; Turnbull, I. M. & Uruski, C., 1993). We suggest that most extension at Parara-1 is of Eocene age.

5.3 Oligocene to early Miocene condensed sequence

SLN2-1 limestone and mudstone was deposited during the Oligocene and early Miocene. Its thickness is ~315 m at the crest of Parara Anticline, and ~250 m just south of the anticline (line M18-17c). We infer that the Parara Fault was active as a normal fault during the late Eocene between ~46 Ma and ~37 Ma (SLN1-1), and then residual accommodation space associated with sediment compaction was filled during a time of generally-low sediment supply (SLN2-1). Significant onlap adjacent to Solander Anticline (Fig. 2B) during deposition of SLN2-1 likely reflects paleo-topography created by earlier fault movement or ongoing fault activity farther west.

5.4 Middle Miocene increase in sediment supply

Biostratigraphic data from Parara-1 indicate a significant increase in mass accumulation rate (MAR) after ~15 Ma (Fig. 5; see Table 2 for NZ Stage ages). The downhole drop in value of the gamma ray log across the top of SLN2-1 probably reflects a downhole increase in carbonate content within the mud-dominated section. SLN2-2 coarsens upward and is sand-dominated in its upper part.

Unit SLN2-2 was deposited from ~15–11 Ma. Strata are parallel across Parara Anticline, indicating that local inversion was not occurring during deposition (Fig. 2B). North of Parara-1, SLN2-2 reaches a maximum thickness of >1200 m, whereas strata are <900 m thick to the south. Thickness variations and basal downlap relationships indicate an increase in sediment supply from the north at ~15 Ma, which is consistent with the regional basin history inferred from stratigraphy immediately east of southern Fiordland (Norris, R. *et al.*, 1978; Norris, R.

& Turnbull, I., 1993; Turnbull, I. M. & Uruski, C., 1993).

5.5 Anticline growth

The base of unit SLN3-1 corresponds to an uphole lithological change from sandstone to mudstone. The top of SLN3-1 corresponds to a mappable reflector that correlates with notable anomalies in gamma ray and resistivity logs. Biostratigraphic data show that the mass accumulation rate (MAR) value was much lower during deposition of SLN3-1 than SLN2-2. Thickness variations and onlap observed on seismic-reflection data (Fig. 2) suggest growth of Parara Anticline during deposition of SLN3-1. Growth of the anticline resulted in local uplift of the Parara-1 site at the anticline crest, resulting in lower local MAR values and channel development adjacent to the flank of the anticline, to where sediment pathways were diverted (see e.g. CDP 13000 on line M18-17c; Fig. 2).

Parara Anticline growth and reconfiguration of sediment distribution pathways occurred during deposition of unit SLN3-1 at ~12-8 Ma (Table 4). Low MAR values at Parara-1 during deposition of SLN3-2 imply that the crest of the anticline remained emergent above the basin-floor depositional system throughout this time interval. It is unclear if faulting persisted during final burial of the anticline (SLN3-2) at ~8-5 Ma, or if thickness variations reflect infilling of topography that was generated during deposition of unit SLN3-1.

5.6 Pliocene-Quaternary

High regional sedimentation rates since ~5 Ma were associated with growth of mountainous source areas in the Southern Alps and Fiordland (Norris, R. & Turnbull, I., 1993; Tippett, J. M. & Kamp, P. J. J., 1993; Sutherland, R., 1996; Sutherland, R. *et al.*, 2009). Megasequence SLN4 was deposited with high MAR values (Fig. 5).

SLN4-1 strata are undeformed at the Parara Anticline relative to underlying strata (with only subtle thinning over the crest of the anticline that is probably related to differential compaction and relic topography) but strata onlap Solander Anticline and thickness variations suggest that growth of Solander Anticline started at ~5 Ma. Ongoing seismic activity, seabed expression, and Quaternary volcanism suggest that reverse activity on the Solander Fault may still be active (Turnbull, I. M. & Uruski, C., 1993; Melhuish, A. *et al.*, 1999; Sutherland, R. *et al.*, 2006).

SLN4-2 was rapidly deposited and has the lowest interval velocities recorded in Parara-1. It represents shelf-slope mudstone deposited at ~2.8-1.9 Ma, before the time of maximum glacial intensity in South Island. SLN4-3 at Parara-1 is the unit associated with late

Quaternary shelf construction.

6 Tauru Fault and SLN to SLS correlation

Tauru High was created by large throw on the Tauru Fault. It is a barrier to sediment transport and stratal continuity, and is the reason for defining separate northern and southern stratigraphic units. We infer the timing of movement on the Tauru Fault based on interpretation of stratigraphy (onlap, thinning, tilting) northeast of Tauru High and ties to Parara-1 (Fig. 6), and hence we correlate between northern and southern sub-basins based on our seismic interpretation of pre-inversion, syn-inversion, and post-inversion southern units.

We identify SLS1-1 in isolated depressions south of the Tauru Fault. We correlate this with units SLN1-1 and SLN2-1, because SLS1-1 reflector geometry suggests it is a rift and post-rift sequence. The thin SLS1-1 correlative for SLN1-1 and SLN2-1 adjacent to the Tauru Fault suggests little accommodation space was available there, possibly due to footwall uplift during Paleogene normal fault movement. Elsewhere in the southern sub-basin, it is unclear how thick correlatives to these older units are, because the top of SLS1-1 is gradational in southern depocentres and is hence difficult to correlate with northern sub-basin units. However, it seems to be much thinner than correlative units mapped near to the coast (Uruski, C. & Turnbull, I., 1990).

Rapid deposition from ~15–12 Ma resulted in a thick (~1 km) SLN2-2 unit north of the Tauru Fault that pre-dates inversion of the Parara Fault. However, SLN2-2 thins against and onlaps Tauru High, suggesting a reversal in topography to that evident in SLN2-1. Early inversion on the Tauru Fault is hence inferred during the period 15-12 Ma, but seabed topography generation was slight, based on the nearly complete coverage of SLN2-2 strata onto Tauru High. Based on thickness in the depocentre north of Tauru High, seismic reflection character (high continuity of reflectors), basal downlap, and stratigraphic position beneath fault-scarp-derived mass-wasting deposits (Fig. 6), we correlate SLS2-1 with SLN2-2.

We interpret the high-amplitude reverse-polarity reflector at the top of SLS2-1 adjacent to the Tauru Fault to be the base of mass-wasting deposits derived from the collapsed fault scarp. We suggest that the event recorded by this reflector is the fault overthrusting the seabed accompanied by collapse of the fault scarp. Initial mass wasting of the growing seabed scarp likely occurred during deposition of SLS2-1 and before large-scale collapse. We infer that inversion of the Tauru Fault continued during deposition of units SLS2-2 and SLS2-3, based on similarities in seismic character and thickness of post-inversion units above and on either side of Tauru High (Fig. 6). Hence, we correlate SLS2-2 and SLS2-3 with SLN3-1, the syn-tectonic inversion unit at Parara Anticline. This is consistent with the establishment of a stable channel system linked to an antecedent gorge that still cuts through Tauru High. We infer that inversion on the Tauru Fault was complete by ∼8 Ma, based on onlap and tilting relationships. Seabed topography persisted during deposition of younger units and a subdued form remains today: Solander Channel remains embedded in a gorge through the barrier. The top of SLN2-1 on Tauru High is at ~2.3 s TWT, but the top of unit SLS1-1 is at ~5.7 s TWT adjacent to Tauru High. Therefore, a total fault throw of ~4.3 km is implied.

7 Depositional mechanisms

7.1 Tasman Sea

Southeast Tasman Ocean Crust (Fig. 1) (Lamarche, G. *et al.*, 1997) has low sediment thickness, even though it is an area of high biological productivity (Jitts, 1964; Hassler et al., 2014) and is adjacent to the mountainous plate boundary zone of South Island. Pelagic sediment accumulates in drifts in shallow (typically <400 m) isolated depressions between abyssal hills and in the lee of minor seamounts (Fig. 7) (Wood, R. A. *et al.*, 1996; Lamarche, G. *et al.*, 1997; Melhuish, A. *et al.*, 1999; Gurnis, M. *et al.*, 2019).

Three factors are responsible for the small sediment thickness. The physiography of the region contains barriers that prevent sediment gravity flows from reaching Southeast Tasman Ocean Crust: Resolution Ridge stops sediment transport from western South Island; and Puysegur Ridge is a barrier to sediment from southern and eastern South Island. The South Tasman abyssal plain is characterized by water depths >4000 m and is close to or beneath the Carbonate Compensation Depth, but the Puysegur trench slope shallows to just 200-700 m depth and rough acoustically-reflective seabed topography (Fig. 7) and seismic-reflection data reveals it is also lacking a significant drape of pelagic sediment (Gurnis, M. *et al.*, 2019). The strong flow of the ACC scours the seabed and transports sediment eastward, meaning that pelagic and hemi-pelagic sediment is swept away from the area. 7), despite high levels of primary productivity near the Subtropical Front (STF) (Chiswell, S. M. *et al.*, 2015).

7.2 Solander shelf and adjacent slope

Strata beneath the present-day continental shelf have characteristic clinoform geometry that downlap a basal surface. These clinoforms exhibit relatively thin upper and lower portions at shallow dips, and a thicker central section (Fig. 8). This shelf configuration implies a combination of high sediment input and relatively static base level. During high-stand conditions the shelf is a sediment reservoir. During low-stand conditions, sediment that previously accumulated on the shelf is reworked to form a new clinoform slope deposit and the rest is transported down Solander Channel by gravity flow mechanisms (Bostock, H. C. *et al.*, 2015).

The continental slope seabed on line M18-17c is characterized by oval pockmarks up to 200 m wide and 10s of m deep (Fig. 8). Pockmarks are inferred to result from fluid escape from strata below (e.g. hydrocarbon, volcanic, or pore fluids). Hovland, M. *et al.* (2002) classify elongate pockmarks based on their asymmetry and suggest they are formed by interaction with strong bottom currents. The observed north-south elongation direction (Fig. 8) is consistent with local southward flow of the STF ~18 km southeast of Solander Island. Gas or fluid associated with Solander Island volcano (Reay, A. & Parkinson, D., 1997) may be a factor, as might hydrothermal dewatering triggered by volcanic heat input or normal burial. Thermal maturation of Eocene or Cretaceous coal measures, which are present in Solander-1 borehole (Shaheen, E. & Hutson, R. J., 1989), may also be a factor.

7.3 Solander Trough

There are two main types of sediment input to Solander Trough: pelagic sediment associated with high biological productivity near the STF; and terrigenous sediment derived from mountain building in the Southern Alps of South Island. Sediment gravity flows move sediment southward down Solander Channel, but the whole region is swept and affected by the STF. Scours and drifts are evident in pelagic and hemi-pelagic settings around structural highs, e.g. in the eastern Snares Zone (Fig. 9A), where southeastward flow is implied by bedforms that show accretion was anchored to topographic barriers that locally divert the STF (Fig. 10A). Deposition of sediment drifts in the northeastern Snares Zone was at a high angle to moating (Fig. 9A), and the lenticular concave-up bedforms (Fig. 10A) can be classified as "elongate mound drifts" (Stow, D. A. *et al.*, 2002). The shelf south of Stewart Island (Fig. 1) has no terrigenous source area and we suggest that it accreted as a series of elongate drifts derived from sediment winnowed from Solander Trough by the STF, i.e. in a similar fashion to the same shelf farther northeast (Lu, H. *et al.*, 2003). The existence of the shelf south of Stewart Island, combined with the lack of sediment on Puysegur Ridge and the Puysegur trench slope suggests that the STF transports fine-grained pelagic and hemi-pelagic sediment eastward out of Solander Trough.

Channel lag deposits or mass transport deposits, probably sandy and pebbly, are inferred from localized high-amplitude reflectors, and allow determination of lateral migration of Solander Channel over time (Figs. 2, 3, 4, & 10B). Growth of seabed topography during Neogene deformation has affected locations of channels by either pushing them sideways (e.g. near Parara Anticline or Solander Anticline) or locking them in position in an antecedent gorge (e.g. Tauru High).

Solander Channel has asymmetric bathymetric expression (Fig. 10B). The western margin of the channel has elevated levee deposits (Fig. 10B). STF flow direction is broadly eastward, and Coriolis deflection of southward moving gravity flows would also be eastward. We propose that as flows try to thin and spread out westward by gravity, they are opposed by these two effects and hence levee aggradation is promoted in a narrow zone of low current velocity west of the main channel. A similar mechanism has been suggested for asymmetric levees adjacent to Bounty Channel, which drains Campbell Plateau eastward (Carter, L. & Carter, R., 1988).

Lateral spreading towards the east of gravity flows centered on Solander Channel is promoted by STF flow and Coriolis effects, resulting in hemi-pelagic deposition that is widely dispersed onto the western slope of Campbell Plateau and towards construction of the shelf south of Stewart Island and eastern South Island (Fig. 1). It is likely that the shelf southeast of Stewart Island is mainly constructed from lateral accretion of sediment drifts, in a similar way to that inferred farther northeast adjacent to South Island (Fulthorpe, C. S. & Carter, R. M., 1991), because there is no other obvious terrigenous sediment source available. Given that Solander Channel activity is mainly restricted to low-stand conditions (Jeromson, M. R., 2016), it is likely that drift accretion to the shelf southeast of Stewart Island is most active during low-stand conditions.

Active erosion by small-scale sediment gravity flows reworks hemi-pelagic and pelagic sediment deposited on the eastern marginal apron of Solander Trough and Campbell Plateau continental slope. Bathymetry reveals erosive canyon features and shelf collapse near the shelf break, slumped material is evident at the foot of the canyon system, and rilled margins of small canyons imply erosion by gravity flows (Fig. 9C). However, seismic-reflection images show that there is net aggradation on the lower part of the slope apron (Fig. 10C). We infer that local sediment gravity flows rework sediment back towards Solander Channel and it aggrades onto the lower continental slope and basin apron.

8 Basin history

Cretaceous rifting was related to separation of Zealandia from Gondwana that led to Tasman seafloor spreading (Gaina, C. *et al.*, 1998; Laird, M. & Bradshaw, J., 2004). Eocene plate boundary reconfiguration resulted in rifting Campbell Plateau from western New Zealand, formation of Emerald Basin, and normal faulting in southern South Island, which was close to the pole of Australia-Pacific relative rotation and hence avoided continental break-up (Turnbull, I. M. & Uruski, C., 1993; Sutherland, R., 1995). Eocene fluvial and lacustrine deposition dominated the onshore region (Turnbull, I. M. & Uruski, C., 1993). Eocene strata in Parara-1 (SLN1-1) are kaolinitic sandstones with coal (Hunt International Petroleum Company 1976). Growth strata against the Parara Fault and Tauru Fault indicate deposition contemporaneous with normal faulting.

Late Eocene and Oligocene deepening is inferred from an upward-fining sequence of turbiditic sands to bioclastic limestone and Oligocene transgression flooded the Fiordland region (Norris, R. & Turnbull, I., 1993; Turnbull, I. M. & Uruski, C., 1993). This sequence of upward fining clastic to carbonate facies is observed onshore in Balleny Basin (Norris, R. & Turnbull, I., 1993), from dredge samples (Sutherland, R. *et al.*, 2006), and at Solander-1 (Engmann, L. A. & Fenton, P. H., 1986). There was a greatly diminished source of terrigenous sediment during the Oligocene, but an active dextral plate boundary near to Fiordland is inferred from regional analysis (Sutherland, R., 1995). Deposition was localised in depocenters associated with prior rifting (Unit SLN1-1).

The early Miocene saw a progressive increase in rate of local plate motion, a shift from local transtension to transpression, and the onset of cooling associated with exhumation of southwestern Fiordland adjacent to Balleny Basin (Sutherland, R., 1995; Sutherland, R. *et al.*, 2009). Oligocene carbonate sequences onshore are overlain by Miocene terrigenous sediment (Norris, R. & Turnbull, I., 1993; Turnbull, I. M. & Uruski, C., 1993). Early Miocene bathyal mudstones were deposited at Parara-1 and Solander-1.

Unit SLN2-1 (35-17 Ma) was deposited near to an active plate boundary, but with only minor sediment sources available. The only evidence for fault activity in Solander Basin during this interval is from onlap of SLN2-1 adjacent to the Solander Fault, which indicates a normal component of throw. Oligocene sedimentation rates were low, and most of the accommodation space was likely generated during the late Eocene to Oligocene.

The Paleogene to early Miocene megasequence south of Tauru High (SLS1) is condensed or missing, and this may be due to a combination of factors: (1) low terrigenous input, due to limited exhumation, and sediment capture in upstream basins, such as Waiau Basin; (2) low primary biological productivity; and (3) the ACC may have been unimpeded by topography and swept any fine-grained sediment eastward, i.e. Puysegur Ridge had not yet formed.

Onshore, early Miocene mudstone is overlain by a diverse mixture of middle and late Miocene mudstone, sandstone, and conglomerate, with a generally coarsening-upward trend recorded in Waiau and Te Anau basins (Norris, R. & Turnbull, I., 1993; Turnbull, I. M. & Uruski, C., 1993). Stratigraphy at Parara-1 shows upward coarsening from mud-dominated to sand and mud (Hunt International Petroleum Company 1976). Solander-1 exhibits upward coarsening from mud to interbedded conglomerate and sand (Engmann, L. A. & Fenton, P. H., 1986). The coarser sediment is inferred to be sourced from uplifted onshore areas, where thermochronology data reveal middle and late Miocene exhumation of western Fiordland (Sutherland, R. *et al.*, 2009).

SLN2-2 was deposited from ~17 Ma to ~12 Ma at a much higher sedimentation rate than SLN2-1 (Fig. 5). Initial inversion of the Tauru Fault is inferred during deposition of SLN2-2, initial uplift of Fiordland occurred at about this time (Sutherland, R. *et al.*, 2009), and plate reconstructions suggest these events were associated with initial growth of Puysegur Ridge (Sutherland, R. *et al.*, 2006). The onset of sedimentation south of Tauru High during this time may be due to combined effects of increased sediment supply and initial growth of Puysegur Ridge, which provided protection from erosion by bottom currents.

Reverse movement on the Parara and Tauru Faults occurred during deposition of SLN3-1 (12-8 Ma), and this forced sediment distribution into channelized pathways between structures. Onshore, the Hump Fault, which is the northern extension of the Solander Fault, was active at about the same time (Turnbull, I. M. & Uruski, C., 1993), but there is no evidence for offshore activity on the Solander or Hauroko Faults at this time (Sutherland, R. *et al.*, 2006). Exhumation was focused in western Fiordland adjacent to the northward propagating subduction thrust (Sutherland, R. *et al.*, 2009).

Late Miocene onshore sediments are characterized by terrestrial deposition (Norris, R. & Turnbull, I., 1993; Turnbull, I. M. & Uruski, C., 1993), and sediment gravity flows transported large quantities of sediment southward down Solander Trough into deep water. At Parara-1 and Solander-1, shelfal muds dominate the late Miocene-earliest Pliocene sequence (Hunt International Petroleum Company 1976; Engmann, L. A. & Fenton, P. H., 1986). Tectonic activity in the offshore basin was relatively minor during deposition of SLS3-2 (8-5 Ma).

During the Pliocene to Pleistocene, uplift spread eastward across Fiordland and glaciers shaped the modern topography (Turnbull, I. M. & Uruski, C., 1993; Sutherland, R. *et al.*, 2009). Solander Island was erupted (Reay, A. & Parkinson, D., 1997) and other subduction-related volcanism included submarine volcanics imaged on seismic data at the southern tip of the Hauroko Fault (Sutherland, R. *et al.*, 2006). Pliocene to Pleistocene sediments at Parara-1 comprise deepwater claystones and siltstones (Hunt International Petroleum Company 1976). The Pliocene-Recent sequence is condensed and not sampled at Solander-1, which is on the crest of an actively-growing anticline (Engmann, L. A. & Fenton, P. H., 1986).

Inversion of the Solander and Hauroko Faults is indicated by seabed topography and onlap of megasequence SLN4 (5-0 Ma). This broadening of the Fiordland segment of the plate boundary is reflected in the exhumation pattern, coastal uplift and regression (Kim, K. & Sutherland, R., 2004; Sutherland, R. *et al.*, 2009). It is likely associated with erosion of the lithosphere in the hanging-wall of the subduction zone and development of space for a slab beneath. We also see evidence for eastward broadening of southern Puysegur Ridge during deposition of SLS3-1 (5-3 Ma), which may also reflect similar process of crustal thickening and lithospheric adjustment to increasing subduction maturity. In contrast, northern Puysegur Ridge and the Snares Zone appear to have undergone Pliocene-Quaternary subsidence, which may reflect weakening of the subduction interface and an increase in slab pull (Gurnis, M. *et al.*, 2019).

9 Conclusions

The first seismic stratigraphic analysis of Solander Trough tied to a borehole was achieved by combining results from the recent MGL1803 2D seismic reflection survey with existing petroleum industry data from the coastal region. Northern and southern sub-basins are separated by the Tauru Fault, which accumulated ~4.3 km of Neogene reverse throw.

The tectonic evolution of Solander Trough reflects the changing stress state during initiation of an oblique subduction zone. We are now able to track the growth of Puysegur Ridge and the intermittent fault activity associated with failure more broadly in the subduction hanging-wall, which reflects evolving forces, space problems, and strength of the main interface. Our data provide a basis for understanding how the general architecture of the stratigraphy is able to track spatial and temporal evolution of the system, and hence future surveying and drilling targets can be identified and our existing and new observations can be used to test geodynamic models.

The stratigraphy of Solander Trough accumulated rapidly since ~17 Ma beneath the STF, and hence may provide unique high-resolution records of Neogene climate influence by both ACC and tropical influences. Sites with mixed hemi-pelagic clay and pelagic carbonate may be resistant to diagenesis and provide ideal material for coring, and hence high-resolution climate records can be used to test climate models.

The sedimentology and basin architecture results from combined effects of tectonics and climate, and can only be understood if both factors are considered simultaneously. Tectonics has generated local accommodation space by fault throw, regional protection from bottom-currents by Puysegur Ridge, and steadily increasing terrigenous sediment supply from mountain building that feeds sediment gravity flows. The changing climate, particularly development of the ACC, has swept the region by bottom currents, affected biological productivity and sea level, and has hence introduced stratigraphic change at a range of different timescales. Our study provides the first framework for understanding Solander Basin architecture, and a strong basis for future work.

Acknowledgements

We thank the Captain and crew of RV Marcus G Langseth. Data were processed using Echos software from Paradigm, and interpreted using Seisware Geophysics. The voyage was funded by the National Science Foundation, USA. MG, JS and EH were supported by NSF grant OCE-1654766. All seismic data will be made available at the Academic Seismic Portal (ASP) at UTIG while all remaining data will be available at the Rolling Deck to Repository (R2R). Editor and reviewers.

Tables

Table 1. Seismic reflection processing sequence

Determine survey geometry and write headers
Trace edit
5-85 Hz Butterworth filter
Resample from 2 to 4 ms
Deconvolution (75 & 24 ms gap, 450 ms operator)
CDP sort (nominal 200 fold)
Velocity model manual picking (2.5 km spacing)
Radon demultiple
Stack
FK migration (and scaled amplitude)

Table 2. Biostratigraphic stage tops at Parara-1, after Hunt International Petroleum Company (1976). Stage name abbreviations and ages from Raine, J. I. *et al.* (2015). Depths are converted from feet below Kelly Bushing (BKB), which was a local rig datum 31.1 m above sea level.

Stage top	Age (Ma)	Depth (m BKB)
Quaternary	0.0	178.6
Wm	2.4	835.2
Wp	3.0	1136.9
Tk	5.3	1557.5
Tt	7.2	1685.5
Sw	11.0	1841.0
Sc	15.1	2572.5
Pl	15.9	2621.3
Po	18.7	2728.0
Lw	21.7	2834.6
Ld	25.2	2920.0
LWh	27.3	2941.3
Ak	34.6	2962.7
Dp	42.6	3148.0
Dt	56.0	3327.8

Table 3. One-way time (OWT) observed checkshot data at Parara-1 (Hunt International Petroleum Company 1976), and calculated two-way time (TWT) below sea level (BSL). Shot horizontal offset was 38.1 m, depth was 10.7 m BSL, and a straight ray path approximation was used.

Depth (m BSL)	**Observed OWT** (s)	**TWT vertical** (ms BSL)
147.8		197
278.9	0.175	361
585.2	0.318	649
887.9	0.472	957
1188.1	0.611	1236
1349.7	0.678	1370
1502.4	0.737	1488
1646.8	0.791	1596
1797.7	0.848	1710
1950.1	0.901	1816
2102.5	0.953	1920
2254.9	1.002	2018
2407.3	1.049	2112
2559.7	1.096	2206
2712.1	1.142	2298
3016.9	1.222	2458
3169.3	1.259	2532
3321.7	1.293	2600
3474.1	1.323	2660
3626.5	1.352	2718
3693.6	1.364	2742

Table 4. Seismic reflectors at Parara-1.

Unit top	**TWT** (ms bsl)	**Depth** (m bkb)	**Age** (Ma)
SLN4-3	197	178.6	0.0
SLN4-2	734	699.8	1.9
SLN4-1	1058	1027.7	2.8
SLN3-2	1445	1477.8	4.9
SLN3-1	1624	1715.0	7.9
SLN2-2	1782	1932.3	11.5
SLN2-1	2240	2647.1	16.6
SLN1-1	2419	2973.7	35.1

Figure captions

Figure 1. Location of Solander Trough (ST), Puysegur Ridge (PR), major faults (red lines) and survey MGL1803 (black bold lines) in southern New Zealand. Other abbreviations: RR, Resolution Ridge; BB, Baleny Basin; HF, Hauroko Fault; SF, Solander Fault; PaF, Parara Fault; SI, Solander Island; TF, Tauru Fault; EB, Eastern Boundary Fault; WB, Western Boundary Fault; SZ, Snares Zone. The relative plate motion vector is the MORVEL model (DeMets, C. *et al.*, 2010). Coloured dots are petroleum boreholes (yellow), and DSDP boreholes (green). The dashed line is Solander Channel, the main gravity flow conduit from South Island to southern Solander Trough.

Figure 2. Seismic reflection profiles through the Parara-1 site, northern sub-basin, with seismic-stratigraphic sequences identified (coloured lines). Bold dashed lines show base of channel axis facies. VE is vertical exaggeration. See Figure 1 for location.

Figure 3. Seismic reflection profiles in the northern part of the southern sub-basin (south of Tauru High), with seismic-stratigraphic sequences identified (coloured lines). Bold dashed lines show base of channel axis facies. VE is vertical exaggeration. See Figure 1 for location.

Figure 4. Seismic reflection profiles in the southern part of the southern sub-basin, with seismic-stratigraphic sequences identified (coloured lines). Bold dashed lines show base of channel axis facies. VE is vertical exaggeration. See Figure 1 for location.

Figure 5. Summary of results from Parara-1 borehole (after Hunt International Petroleum Company 1976). New Zealand (NZ) stages and ages after (Raine, J. I. *et al.*, 2015). Mass accumulation rate (MAR) calculated from Table 2 and compaction parameters for Taranaki mudstone (Funnell, R. H. & Allis, R. G., 1996). Interval velocities calculated from checkshot survey (Table 3). Reflector depths from Table 4. See Figure 1 for location.

Figure 6. Cartoon showing evolution of Tauru Fault and stratigraphic correlation. VE is vertical exaggeration. See Figure 1 for location.

Figure 7. Perspective view of (A) Solander Trough, Puysegur Ridge, Puysegur Trench and Tasman Abyssal Plain; with close-ups of (B) northern Puysegur Ridge, and (C) southern Puysegur Ridge, that illustrate rough seabed topography of the abyssal plain (fracture zones and abyssal hills), and the trench slope. The contrast in seabed morphology between the smoother and shallower Solander Trough seabed that is characterized by channels, levees and drifts; and the rough topography of the trench-slope and abyssal plain demonstrates how low sediment supply and strong bottom currents sweep the seabed west of Puysegur Ridge, and

concentrate sediment into Solander Trough.

Figure 8. A, Swath bathymetry data from the continental slope near the Parara-1 site. B, Seismic reflection data across the pockmarks. C, Seismic reflection profile across the shelf at the Parara-1 site. VE is vertical exaggeration. See Figure 1 for location.

Figure 9. Swath bathymetry data from a transect across Solander Trough from the Snares Zone (A), to the central basin axis and Solander Channel (B), and the western slope of Campbell Plateau (C). See Figure 1 for location.

Figure 10. Seismic reflection profiles corresponding to locations shown in Figure 9, with stratigraphic interpretation annotated. VE is vertical exaggeration.

10 References

BARKER, P.F., FILIPPELLI, G.M., FLORINDO, F., MARTIN, E.E. & SCHER, H.D. (2007) Onset and Role of the Antarctic Circumpolar Current. *Deep Sea Research Part II: Topical Studies in Oceanography*, **54,** 2388-2398.

BOSTOCK, H., JENKINS, C., MACKAY, K., CARTER, L., NODDER, S., ORPIN, A., PALLENTIN, A. & WYSOCZANSKI, R. (2019) Distribution of Surficial Sediments in the Ocean around New Zealand/Aotearoa. Part A: Continental Slope and Deep Ocean. *New Zealand Journal of Geology and Geophysics*, **62,** 1-23.

BOSTOCK, H.C., HAYWARD, B.W., NEIL, H.L., SABAA, A.T. & SCOTT, G.H. (2015) Changes in the Position of the Subtropical Front South of New Zealand since the Last Glacial Period. *Paleoceanography*, **30,** 824-844.

CARTER, L. & CARTER, R. (1988) Late Quaternary Development of Left-Bank-Dominant Levees in the Bounty Trough, New Zealand. *Marine Geology*, **78,** 185-197.

CARTER, L., CARTER, R.M., MCCAVE, I.N. & GAMBLE, J. (1996) Regional Sediment Recycling in the Abyssal Southwest Pacific Ocean. *Geology*, **24,** 735-738.

CARTER, L. & MCCAVE, I. (1997) The Sedimentary Regime beneath the Deep Western Boundary Current Inflow to the Southwest Pacific Ocean. *Journal of Sedimentary Research*, **67,** 1005-1017.

CARTER, L., MCCAVE, I. & WILLIAMS, M.J. (2008) Circulation and Water Masses of the Southern Ocean: A Review. *Developments in earth and environmental sciences*, **8,** 85-114.

CARTER, R., MCCAVE, I. & CARTER, L. (2004) Leg 181 Synthesis: Fronts, Flows, Drifts, Volcanoes, and the Evolution of the Southwestern Gateway to the Pacific Ocean, Eastern New Zealand. *Proceedings of the Ocean Drilling Program: scientific results*, **181,** 1-111.

CASTILLO, P.R. (2012) Adakite Petrogenesis. *Lithos*, **134,** 304-316.

CATUNEANU, O., ABREU, V., BHATTACHARYA, J., BLUM, M., DALRYMPLE, R., ERIKSSON, P., FIELDING, C.R., FISHER, W.L., GALLOWAY, W.E. & GIBLING, M. (2009) Towards the Standardization of Sequence Stratigraphy. *Earth-Science Reviews*, **92,** 1-33.

CHISWELL, S.M., BOSTOCK, H.C., SUTTON, P.J. & WILLIAMS, M.J. (2015) Physical Oceanography of the Deep Seas around New Zealand: A Review. *New Zealand Journal of Marine and Freshwater Research*, **49,** 286-317.

COLLOT, J.-Y., LAMARCHE, G., WOOD, R., DELTEIL, J., SOSSON, M., LEBRUN, J.-F. & COFFIN, M. (1995) Morphostructure of an Incipient Subduction Zone Along a Transform Plate Boundary: Puysegur Ridge and Trench. *Geology*, **6,** 519-522.

DEACON, G. (1982) Physical and Biological Zonation in the Southern Ocean. *Deep Sea Research*

Part A. Oceanographic Research Papers, **29,** 1-15.

DeMets, C., Gordon, R.G. & Argus, D.F. (2010) Geologically Current Plate Motions. *Geophysical Journal International*, **181,** 1-80.

Eberhart-Phillips, D. & Reyners, M. (2001) A Complex, Young Subduction Zone Imaged by Three-Dimensional Seismic Velocity, Fiordland, New Zealand. *Geophysical Journal International*, **146,** 731-746.

Engmann, L.A. & Fenton, P.H. (1986) Well Completion Report. Solander-1. Ppl 38206, Technical report, Ministry of Economic Development.

Fulthorpe, C.S. & Carter, R.M. (1991) Continental-Shelf Progradation by Sediment-Drift Accretion. *Geological Society of America Bulletin*, **103,** 300-309.

Funnell, R.H. & Allis, R.G. (1996). *Hydrocarbon Maturation Potential of Offshore Canterbury and Great South Basins*. 1996 New Zealand Petroleum Conference, Ministry of Commerce, Wellington, N.Z.

Gaina, C., Müller, D.R., Royer, J.Y., Stock, J., Hardebeck, J. & Symonds, P. (1998) The Tectonic History of the Tasman Sea: A Puzzle with 13 Pieces. *Journal of Geophysical Research: Solid Earth*, **103,** 12413-12433.

Gurnis, M., Hall, C.E. & Lavier, L.L. (2004) Evolving Force Balance During Incipient Subduction. *Geochemistry, Geophysics, Geosystems*, **5,** Q07001, doi:07010.01029/02003GC000681.

Gurnis, M., Van Avendonk, H., Gulick, S.P., Stock, J., Sutherland, R., Hightower, E., Shuck, B., Patel, J., Williams, E. & Kardell, D. (2019) Incipient Subduction at the Contact with Stretched Continental Crust: The Puysegur Trench. *Earth and Planetary Science Letters*, **520,** 212-219.

Hassler, C.S., Ridgway, K.R., Bowie, A., Butler, E., Clementson, L., Doblin, M., Davies, D.M., Law, C., Ralph, P.J. & Van der Merwe, P. (2014) Primary Productivity Induced by Iron and Nitrogen in the Tasman Sea: An Overview of the Pints Expedition. *Marine and Freshwater Research*, **65,** 517-537.

House, M.A., Gurnis, M., Kamp, P.J.J. & Sutherland, R. (2002) Uplift in the Fiordland Region, New Zealand; Implications for Incipient Subduction. *Science*, **297,** 2038-2041.

Hovland, M., Gardner, J.V. & Judd, A. (2002) The Significance of Pockmarks to Understanding Fluid Flow Processes and Geohazards. *Geofluids*, **2,** 127-136.

Hunt International Petroleum Company (1976) Well Completion Report Parara-1, Technical report, Ministry of Economic Development.

Jeromson, M.R. (2016) The Distribution and Characteristics of Turbidites in the Solander Trough, South of New Zealand, University of Auckland, University of Auckland.

Jitts, H. (1965) The Summer Characteristics of Primary Productivity in the Tasman and Coral Seas. *Marine and Freshwater Research*, **16,** 151-162.

Kennett, J.P. (1977) Cenozoic Evolution of Antarctic Glaciation, Circum-Antarctic Ocean, and Their Impact on Global Paleoceanography. *Journal of Geophysical Research-Oceans and Atmospheres*, **82,** 3843-3860.

Kim, K. & Sutherland, R. (2004) Uplift Rate and Landscape Development in Southwest Fiordland, New Zealand, Determined Using 10be and 26al Exposure Dating of Marine Terraces. *Geochimica et Cosmochimica Acta*, **68,** 2313-2319.

Klepeis, K., Webb, L., Blatchford, H., Jongens, R., Turnbull, R. & Schwartz, J. (2019) The Age and Origin of Miocene-Pliocene Fault Reactivations in the Upper Plate of an Incipient Subduction Zone, Puysegur Margin, New Zealand. *Tectonics*, **38,** 3237-3260.

Laird, M. & Bradshaw, J. (2004) The Break-up of a Long-Term Relationship: The Cretaceous Separation of New Zealand from Gondwana. *Gondwana Research*, **7,** 273-286.

Lamarche, G., Collot, J.Y., Wood, R.A., Sosson, M., Sutherland, R. & Delteil, J. (1997) The Oligocene-Miocene Pacific-Australia Plate Boundary, South of New Zealand: Evolution from Oceanic Spreading to Strike-Slip Faulting. *Earth and Planetary Science*

Letters, **148,** 129–139.

Lamarche, G. & Lebrun, J.-F. (2000) Transition from Strike-Slip Faulting to Oblique Subduction: Active Tectonics at the Puysegur Margin, South New Zealand. *Tectonophysics*, **316,** 67-89.

Lorrey, A.M., Vandergoes, M., Almond, P., Renwick, J., Stephens, T., Bostock, H., Mackintosh, A., Newnham, R., Williams, P.W. & Ackerley, D. (2012) Palaeocirculation across New Zealand During the Last Glacial Maximum at~ 21 Ka. *Quaternary Science Reviews*, **36,** 189-213.

Lu, H., Fulthorpe, C.S. & Mann, P. (2003) Three-Dimensional Architecture of Shelf-Building Sediment Drifts in the Offshore Canterbury Basin, New Zealand. *Marine Geology*, **193,** 19-47.

McCave, I., Carter, L. & Hall, I.R. (2008) Glacial–Interglacial Changes in Water Mass Structure and Flow in the Sw Pacific Ocean. *Quaternary Science Reviews*, **27,** 1886-1908.

Melhuish, A., Sutherland, R., Davey, F.J. & Lamarche, G. (1999) Crustal Structure and Neotectonics of the Puysegur Oblique Subduction Zone, New Zealand. *Tectonophysics*, **313,** 335-362.

Mortimer, N., Gans, P., Foley, F., Turner, M., Daczko, N., Robertson, M. & Turnbull, I. (2013) Geology and Age of Solander Volcano, Fiordland, New Zealand. *The Journal of Geology*, **121,** 475-487.

Norris, R., Carter, R. & Turnbull, I. (1978) Cainozoic Sedimentation in Basins Adjacent to a Major Continental Transform Boundary in Southern New Zealand. *Journal of the Geological Society*, **135,** 191-205.

Norris, R. & Turnbull, I. (1993) Cenozoic Basins Adjacent to an Evolving Transform Plate Boundary, Southwest New Zealand. *South Pacific Sedimentary Basins. Sedimentary Basins of the World. Amsterdam, Elsevier Science Publishers BV*, 251-270.

Raine, J.I., Beu, A.G., Boyes, A.F., Campbell, H., Cooper, R.A., Crampton, J.S., Crundwell, M.P., Hollis, C.J. & Morgans, H. (2015) *Revised Calibration of the New Zealand Geological Timescale: Ntgt2015/1.* GNS Science Lower Hutt.

Reay, A. & Parkinson, D. (1997) Adakites from Solander Island, New Zealand. *New Zealand Journal of Geology and Geophysics*, **40,** 121-126.

Rintoul, S., Hughes, C. & Olbers, D. (2001) The Antarctic Circumpolar Current System. *In: Ocean Circulation and Climate/G. Siedler, J. Church and J. Gould, eds. New York: Academic Press. p.*, 271-302.

Schuur, C.L., Coffin, M.F., Frohlich, C., Massell, C.G., Karner, G.D., Ramsay, D. & Caress, D.W. (1998) Sedimentary Regimes at the Macquarie Ridge Complex: Interaction of Southern Ocean Circulation and Plate Boundary Bathymetry. *Paleoceanography*, **13,** 646-670.

Shaheen, E. & Hutson, R.J. (1989) Petroleum Report 1489: Stratigraphic and Structural Interpretation Using Seismic Attribute Processing. Ppl38206, Solander Basin, South Island, New Zealand, Technical report, Ministry of Economic Development.

Smith, R.O., Vennell, R., Bostock, H.C. & Williams, M.J. (2013) Interaction of the Subtropical Front with Topography around Southern New Zealand. *Deep Sea Research Part I: Oceanographic Research Papers*, **76,** 13-26.

Stow, D.A., Faugères, J.-C., Howe, J.A., Pudsey, C.J. & Viana, A.R. (2002) Bottom Currents, Contourites and Deep-Sea Sediment Drifts: Current State-of-the-Art. *Geological Society, London, Memoirs*, **22,** 7-20.

Sutherland, R. (1995) The Australia-Pacific Boundary and Cenozoic Plate Motions in the Sw Pacific: Some Constraints from Geosat Data. *Tectonics*, **14,** 819-831.

Sutherland, R. (1996) Transpressional Development of the Australia-Pacific Boundary through Southern South Island, New Zealand: Constraints from Miocene-Pliocene Sediments, Waiho-1 Borehole, South Westland. *New Zealand journal of geology and geophysics*,

39, 251-264.

SUTHERLAND, R. & MELHUISH, A. (2000) Formation and Evolution of the Solander Basin, Southwestern South Island, New Zealand, Controlled by a Major Fault in Continental Crust and Upper Mantle. *Tectonics*, **19,** 44-61.

SUTHERLAND, R., BARNES, P. & URUSKI, C. (2006) Miocene-Recent Deformation, Surface Elevation, and Volcanic Intrusion of the Overriding Plate During Subduction Initiation, Offshore Southern Fiordland, Puysegur Margin, Southwest New Zealand. *New Zealand Journal of Geology and Geophysics*, **49,** 131-149.

SUTHERLAND, R., GURNIS, M., KAMP, P.J. & HOUSE, M.A. (2009) Regional Exhumation History of Brittle Crust During Subduction Initiation, Fiordland, Southwest New Zealand, and Implications for Thermochronologic Sampling and Analysis Strategies. *Geosphere*, **5,** 409-425.

TIPPETT, J.M. & KAMP, P.J.J. (1993) Fission Track Analysis of the Late Cenozoic Vertical Kinematics of Continental Pacific Crust, South Island, New Zealand. *Journal of Geophysical Research*, **98,** 16,119-116,148.

TURNBULL, I.M. & URUSKI, C. (1993) Cretaceous and Cenozoic Sedimentary Basins of Western Southland, South Island, New Zealand. *Monogr./Inst. of geol. and nuclear sciences*.

TURNBULL, I.M., ALLIBONE, A.H. & JONGENS, R. (2010) *Geology of the Fiordland Area : Scale 1:250,000*. GNS Science, Lower Hutt.

URUSKI, C. & TURNBULL, I. (1990) Stratigraphy and Structural Evolution of the West Southland Sedimentary Basins. *1989 New Zealand Oil Exploration Proceedings***,** 225-240.

VAIL, P., MITCHUM JR, R. & THOMPSON III, S. (1977) Seismic Stratigraphy and Global Changes of Sea Level: Part 4. Global Cycles of Relative Changes of Sea Level.: Section 2. Application of Seismic Reflection Configuration to Stratigraphic Interpretation. *American Association of Petroleum Geolists Memoir*, **26,** 83-97.

WOOD, R.A., LAMARCHE, G., HERZER, R.H., DELTEIL, J. & DAVY, B. (1996) Paleogene Seafloor Spreading in the Southeast Tasman Sea. *Tectonics*, **15,** 966-975.

Stratigraphic architecture of Solander Trough records Southern Ocean currents and subduction initiation beneath southwest New Zealand

Figures

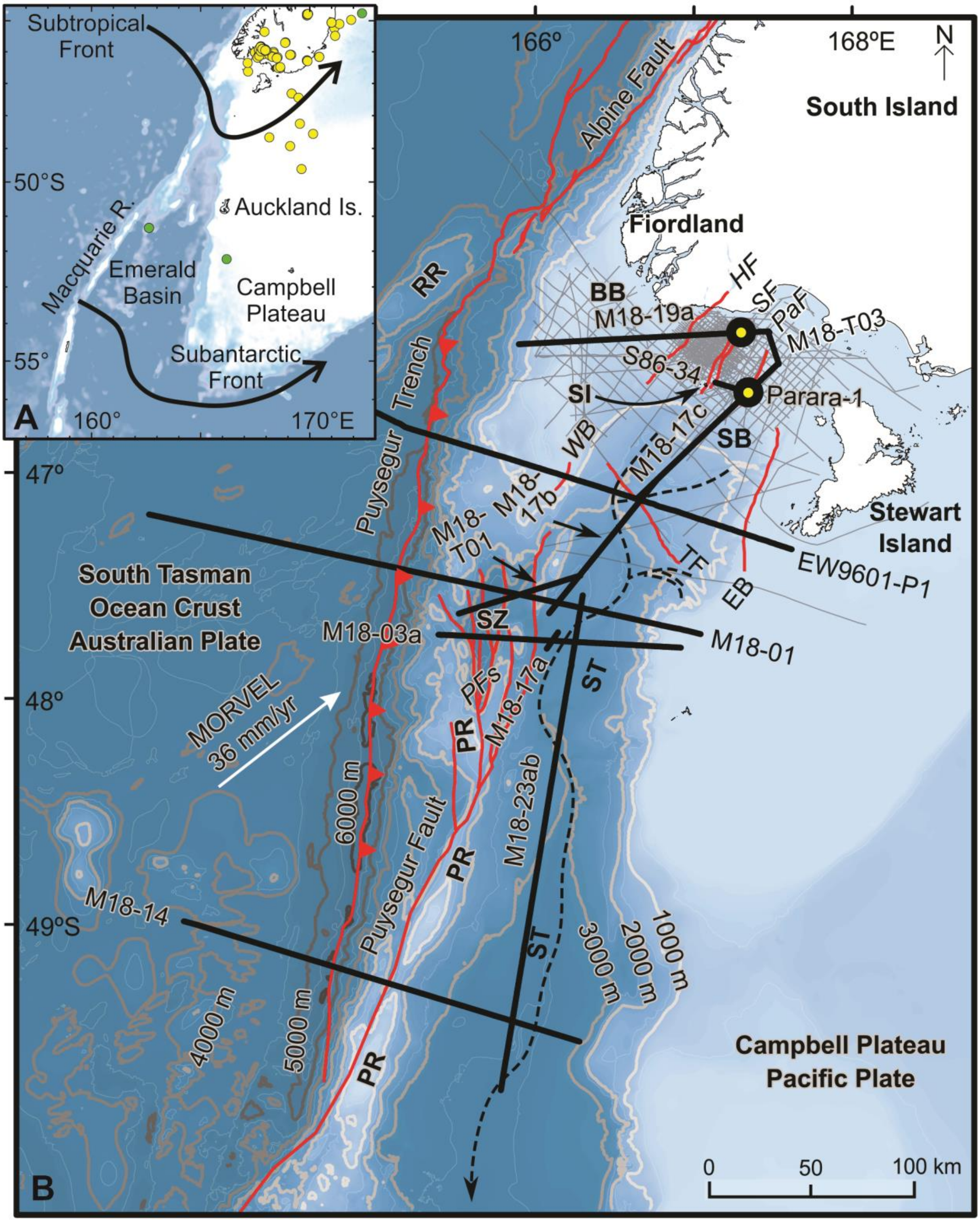

Fig. 1. Location.

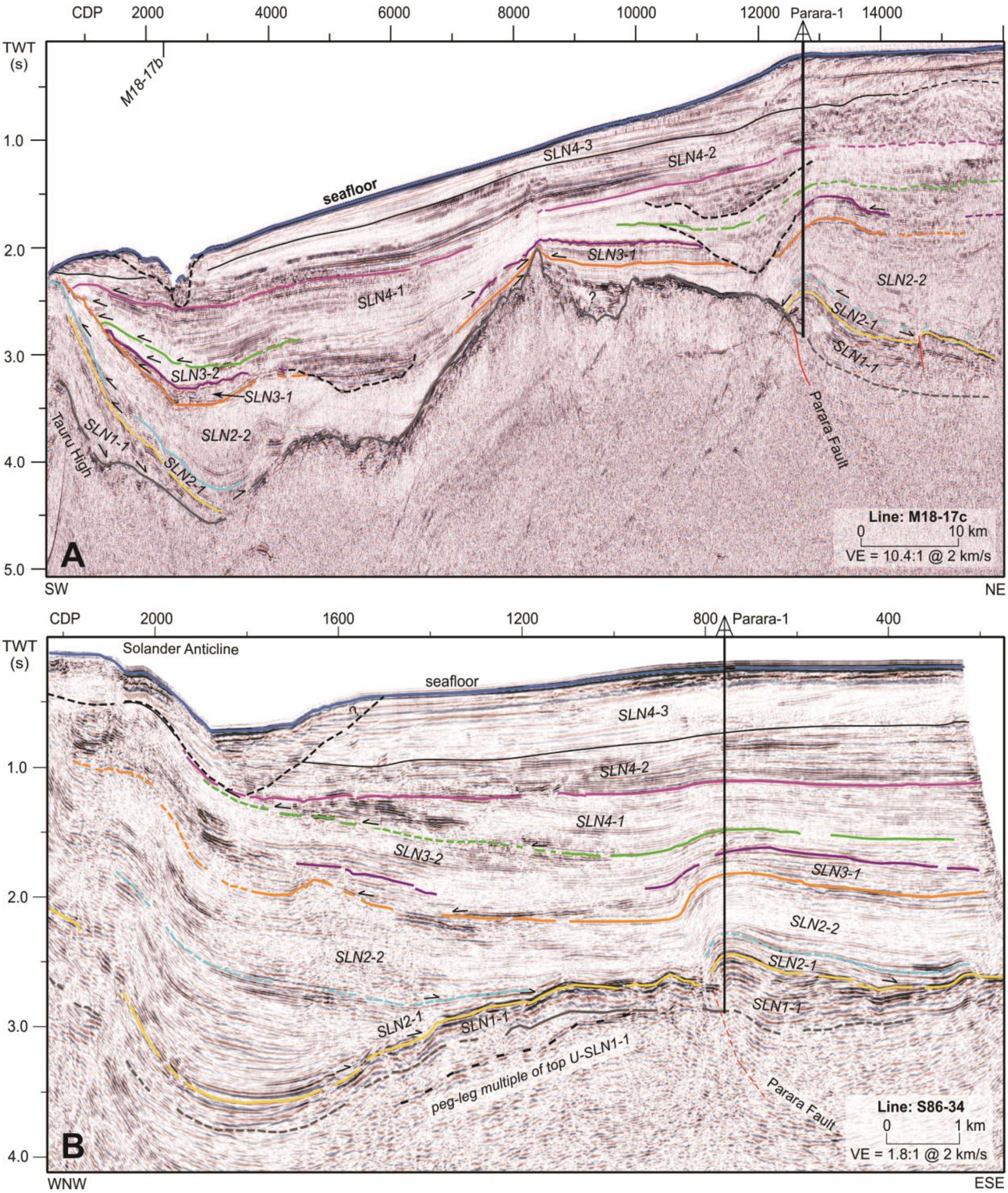

Fig. 2. SLN near Parara-1.

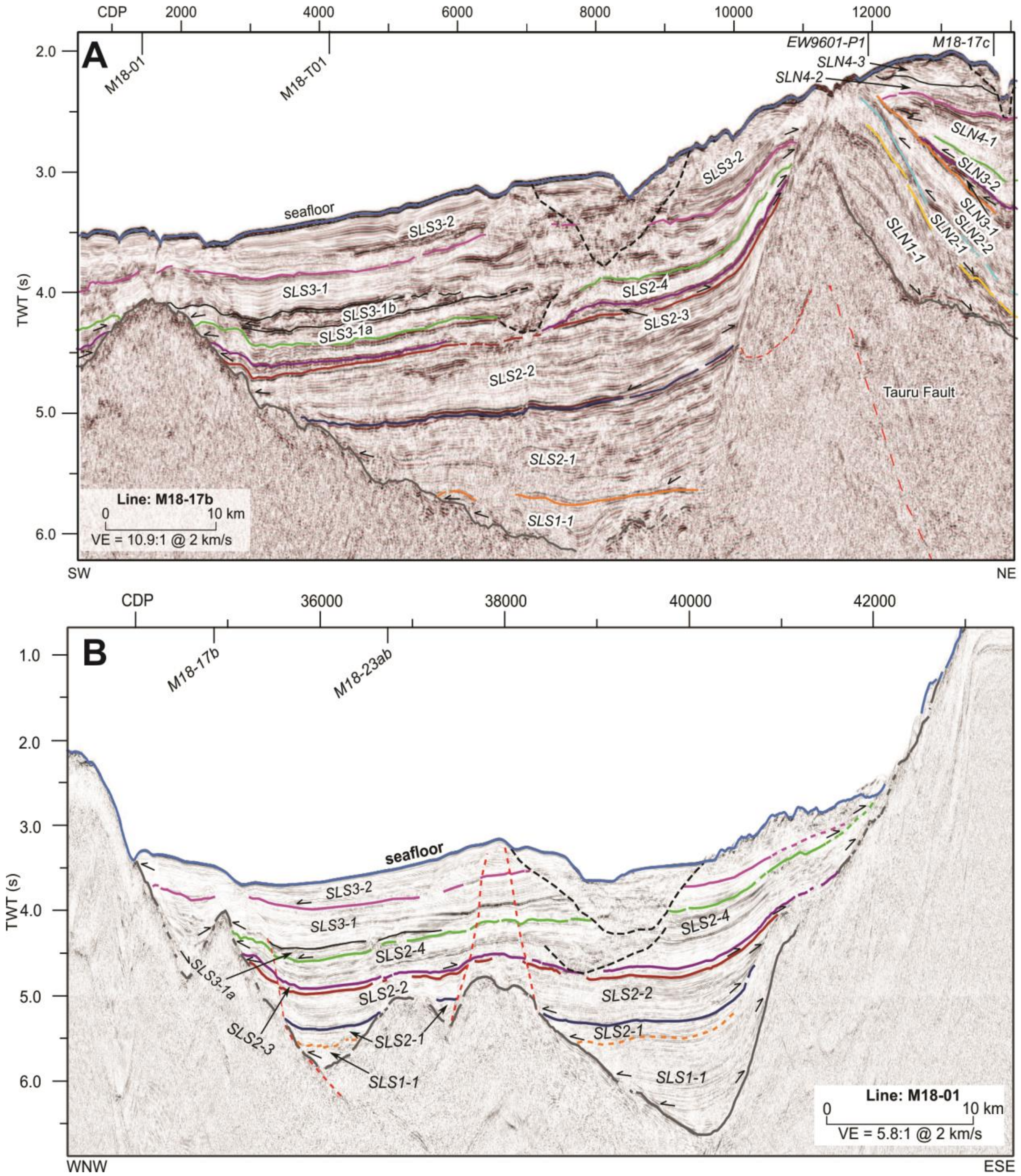

Fig. 3. Tauru Fault and northern SLS.

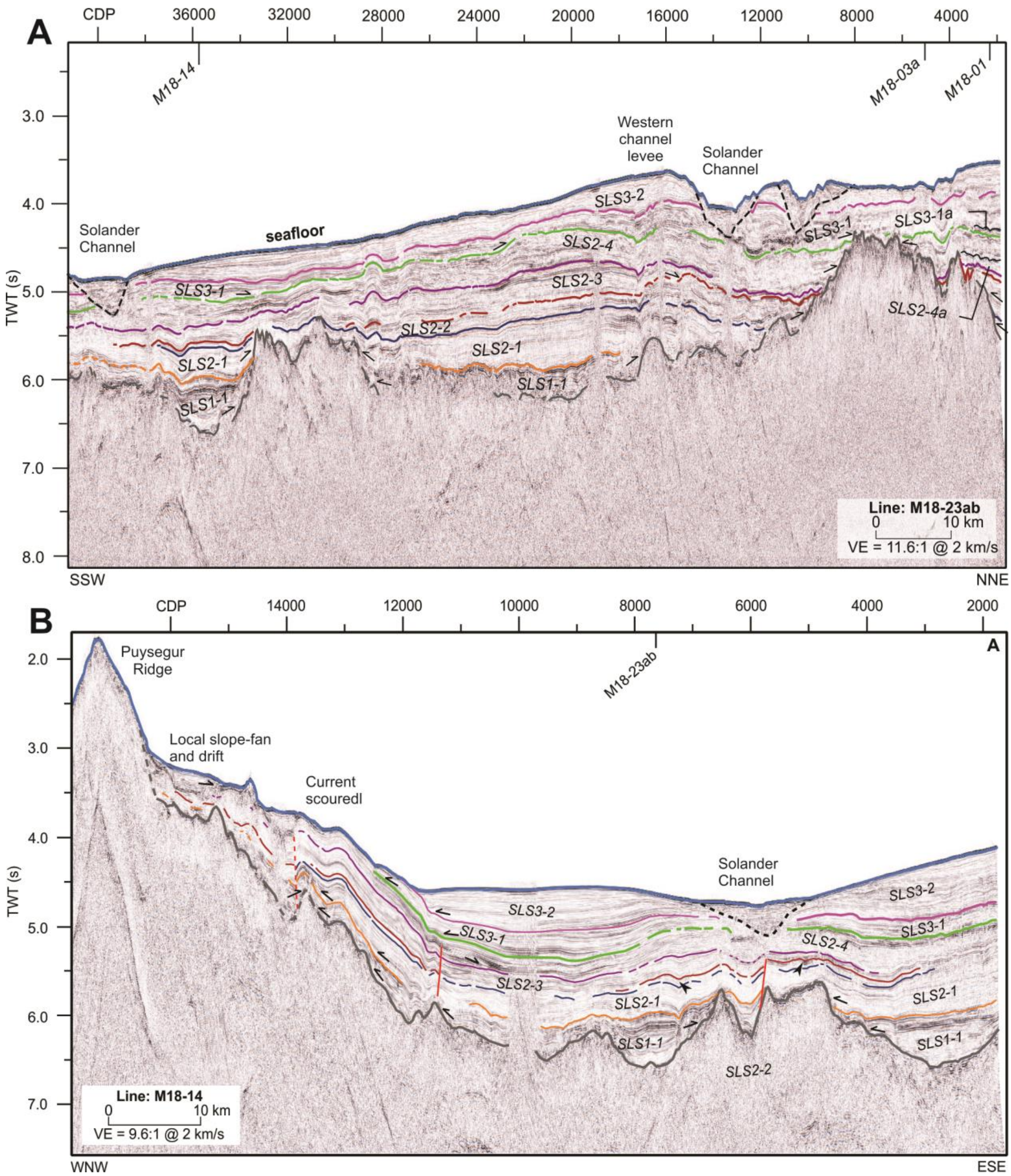

Fig. 4. Southern SLS.

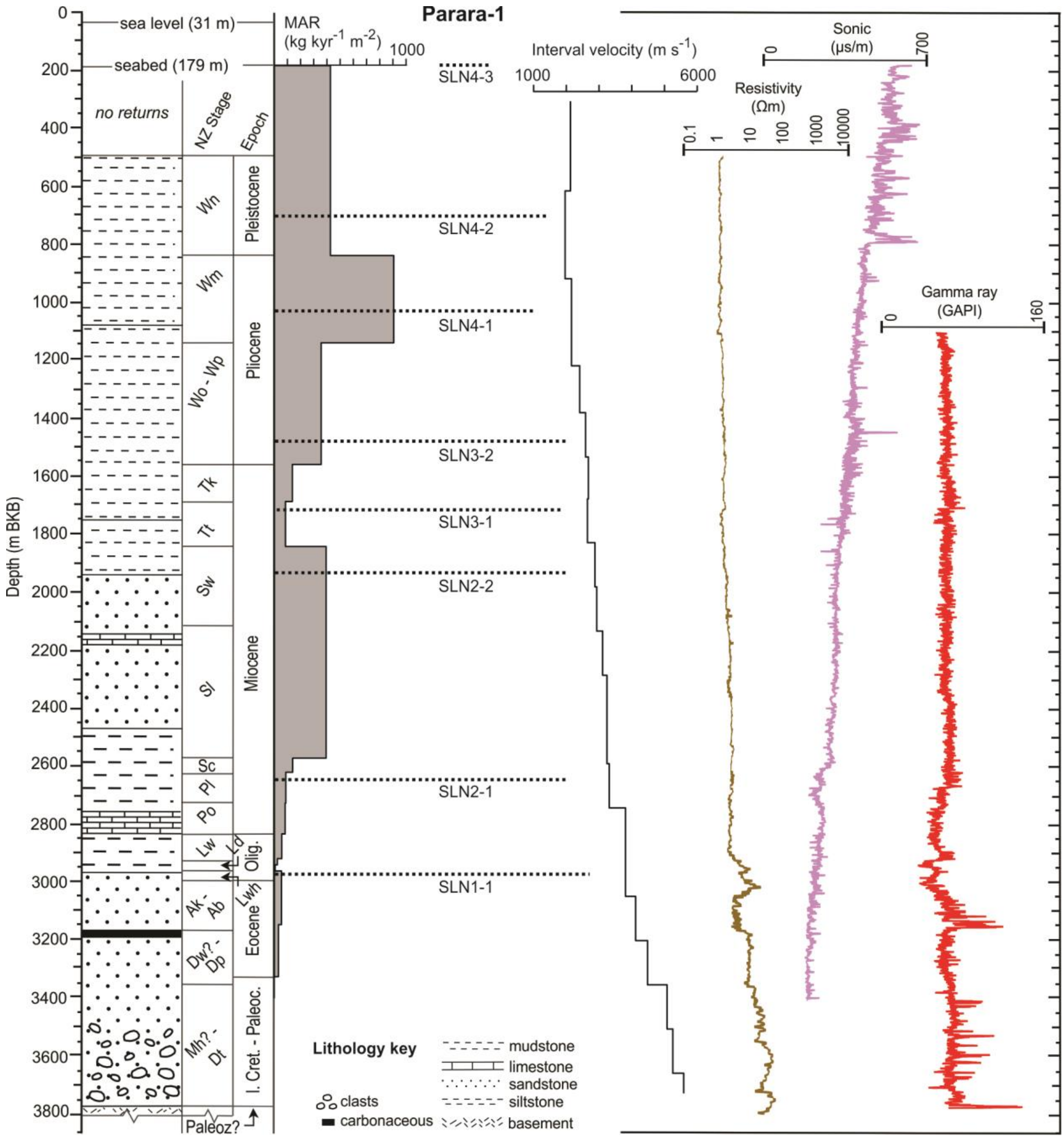

Fig. 5. Parara-1 well.

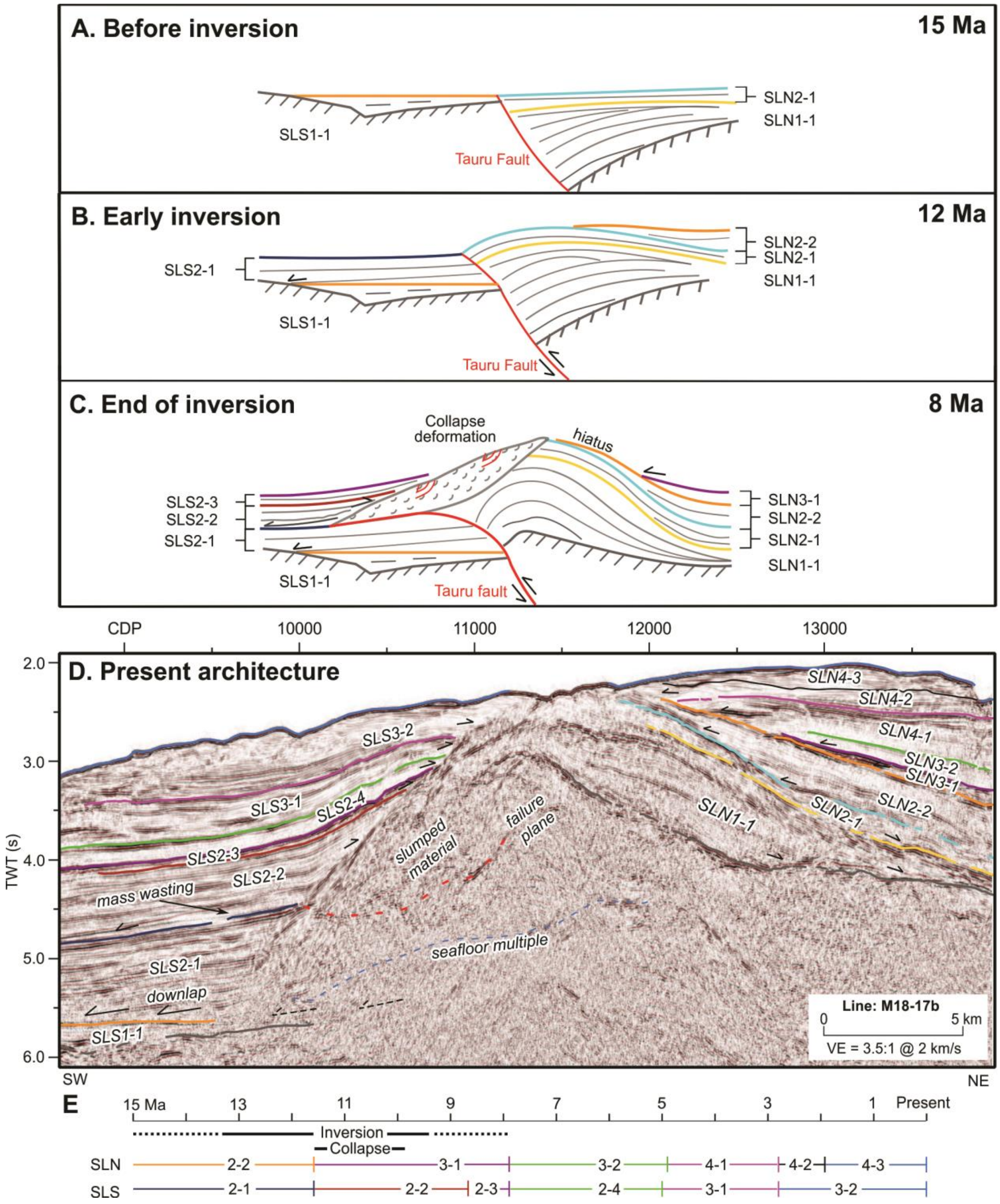

Fig. 6. Tauru Fault evolution and correlation across it.

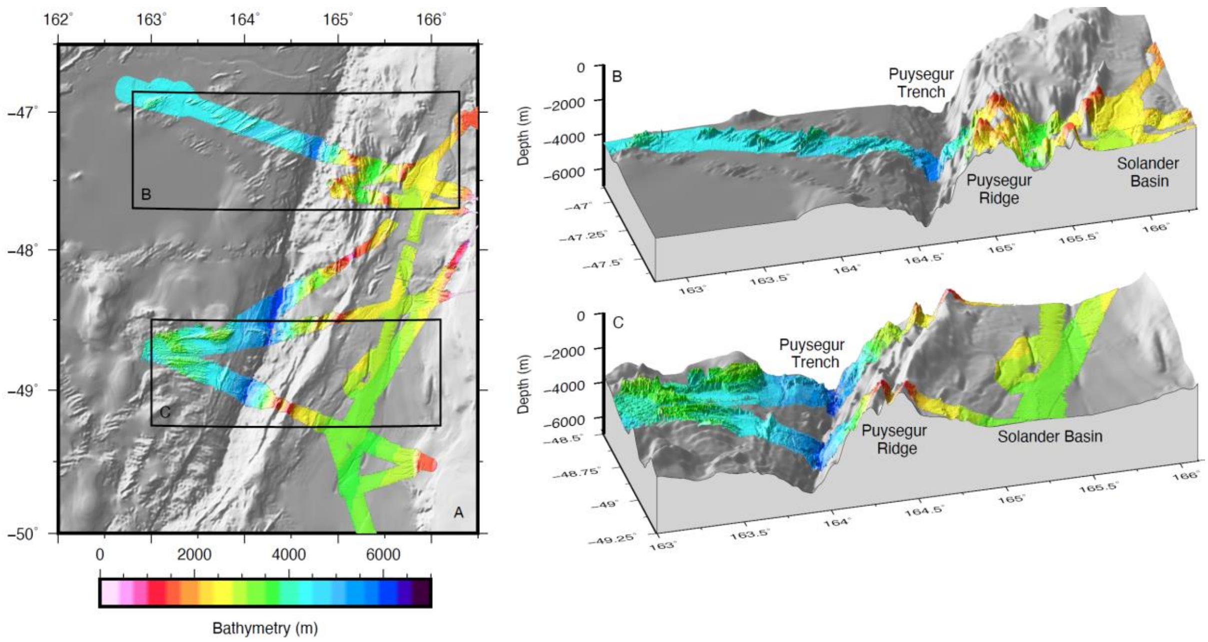

Fig. 7. Tasman abyssal plain, Puysegur Trench and Ridge.

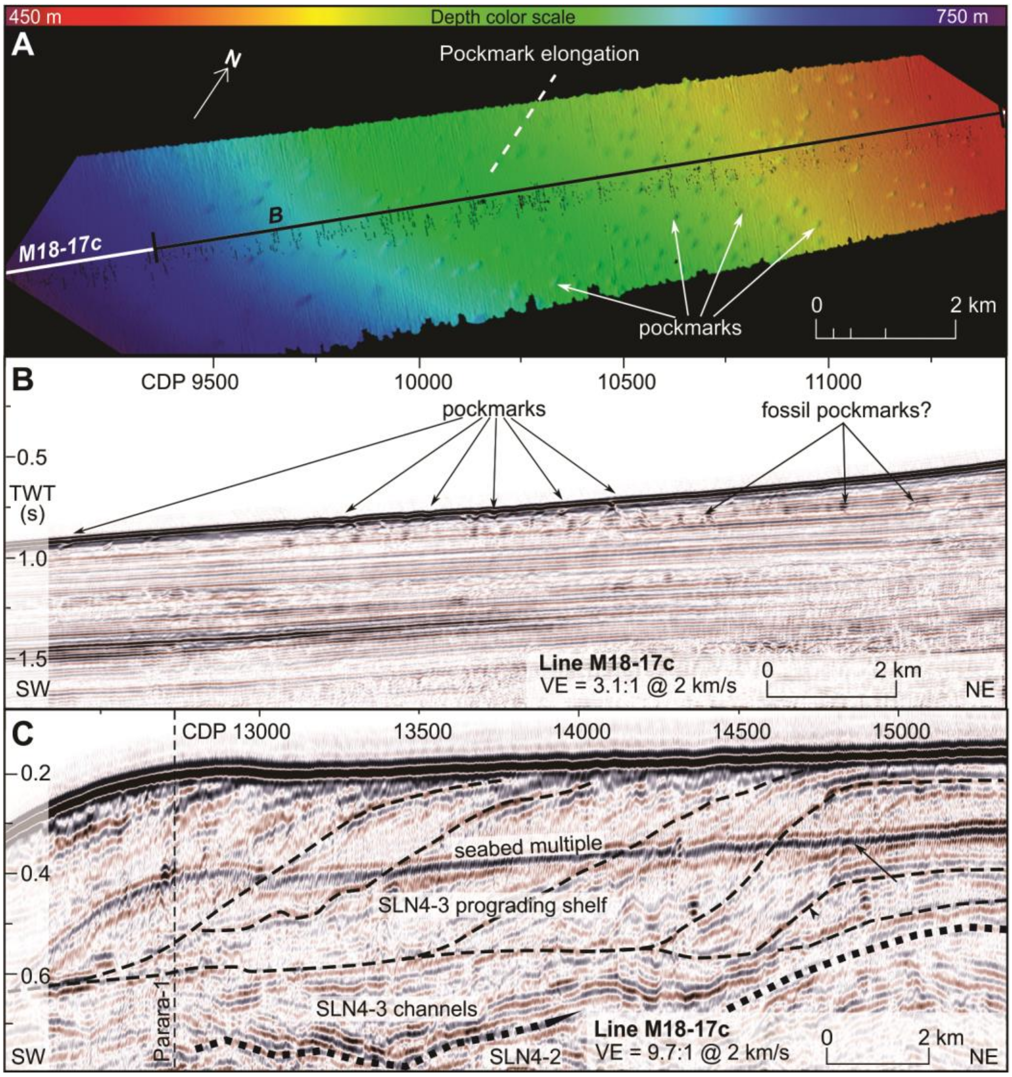

Fig. 8. Pockmarks on the shelf-slope and clinoforms beneath the shelf.

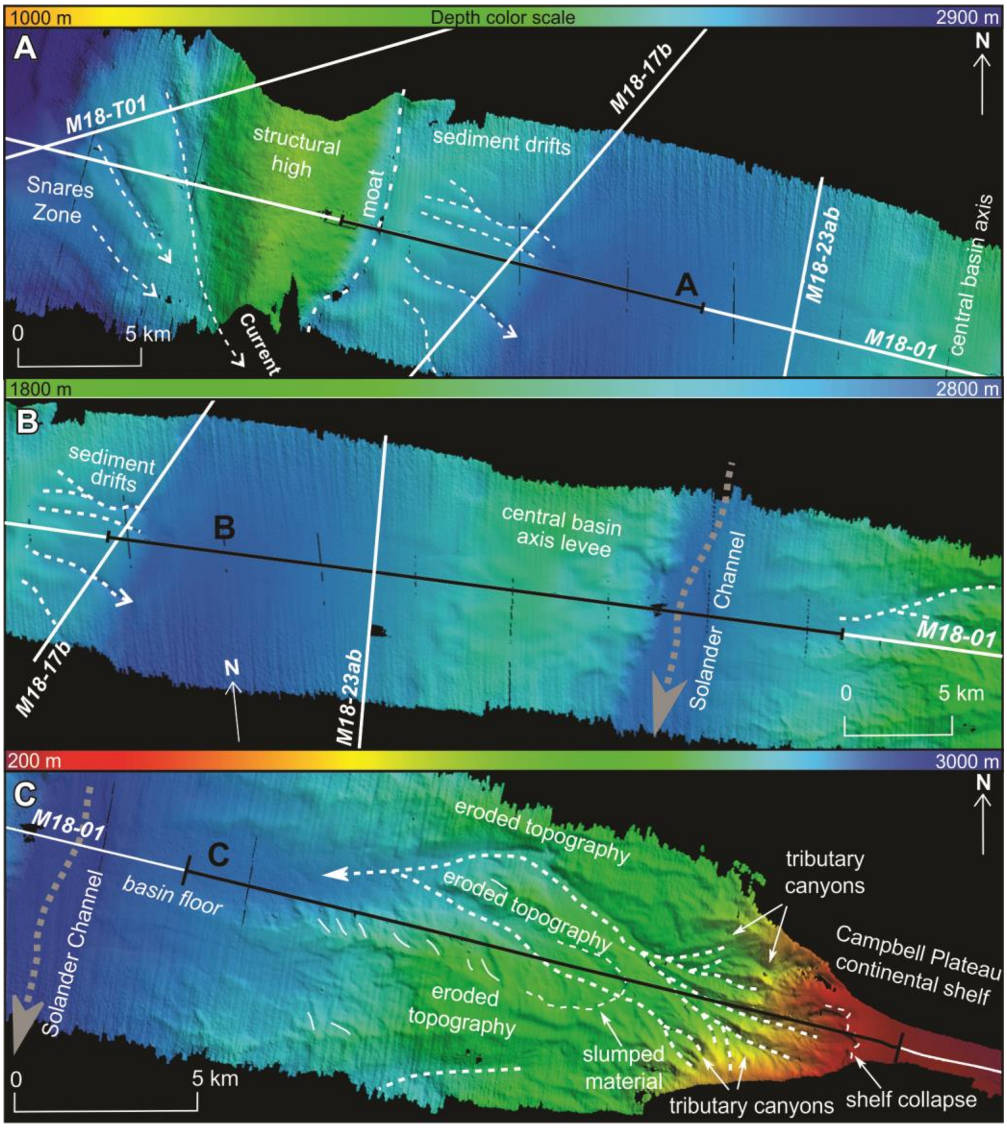

Fig. 9. M18-01 sedimentological interpretation of swath bathymetry data, southern Solander Trough.

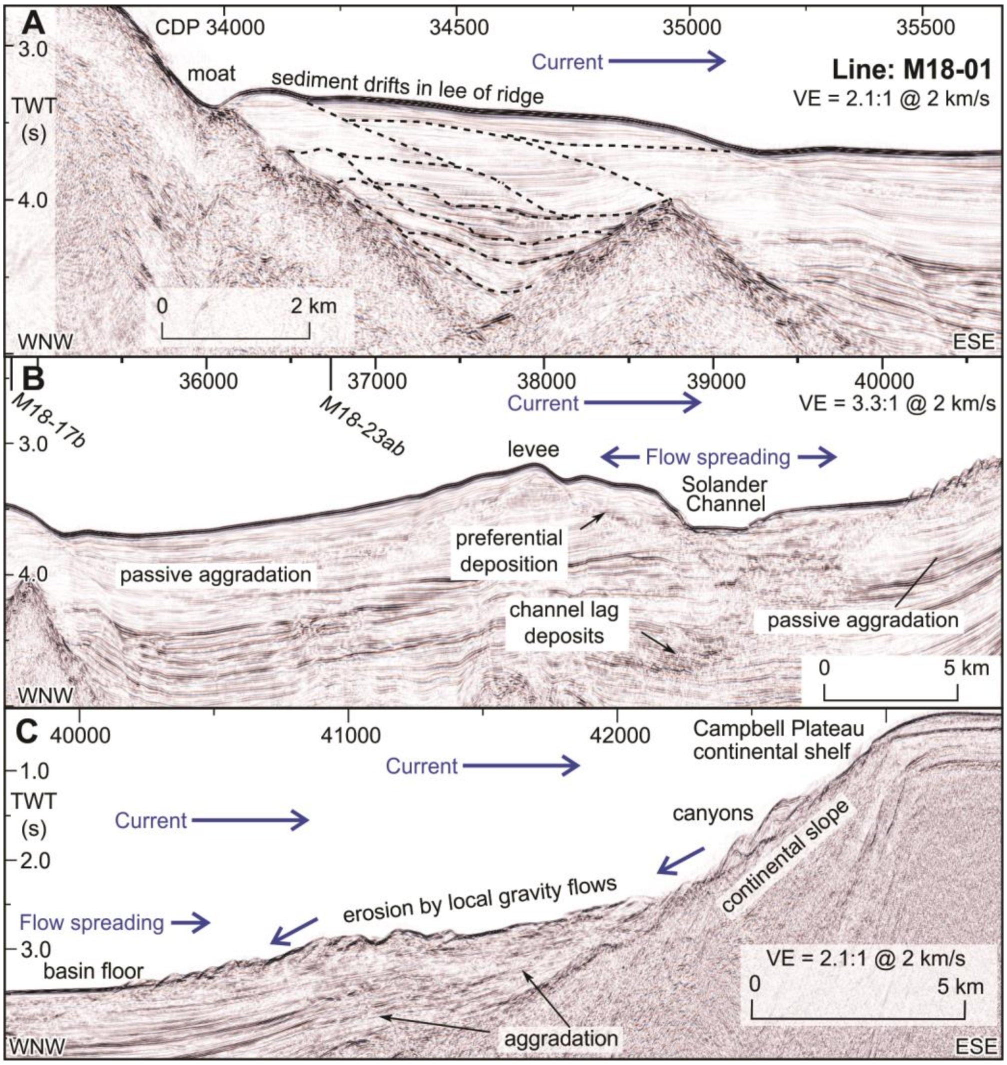

Fig. 10. M18-01 sedimentological interpretation of MCS data, southern Solander Trough.